REVIEW

Solar−Thermal Water Evaporation: A Review

Yunsong Pang, Jiajia Zhang, Ruimin Ma, Zhiguo Qu,* Eungkyu Lee,* and Tengfei Luo*
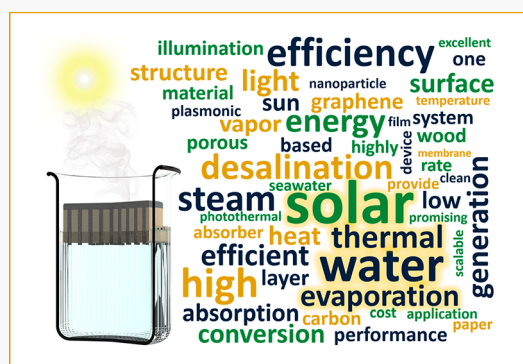
Read Online

ACCESS | Metrics & More | Article Recommendations

ABSTRACT: Solar−thermal water evaporation (SWE) has received much interest in recent years due to a few seminal works on materials innovation and thermal management. With many studies proposing applications like water desalination and sanitization, SWE has become attractive as it can use renewable energy to potentially address pressing water−energy nexus challenges. In this Review, we follow the most researched aspects of SWE indicated by the analytics from text mining the abstracts of papers in this field. We review recent research activities in each aspect and discuss how these studies help improve the overall efficiency of the SWE processes and/or advance their applications, besides pointing out critical deficiencies in the research. We also highlight some interesting findings and inventions emerging from this field. On the basis of the review, we present our perspectives from the scientific and engineering points of view in the hope of providing insights to shape the research direction of the field, promote its further advancement, and eventually help realize the promised applications.

olar−thermal water evaporation (SWE), as an essential part of the natural water cycle, has also been utilized for different applications, such as water boiling in concentrated solar towers for electricity generation,[1] water stills,[2−5] and superheated vapor generation for sanitization.[6] In recent years, thanks to two seminal works from the Halas group[7] and the Chen group,[8] SWE with no or low optical concentration has attracted revitalized attention because it displayed interesting fundamental physics and has attractive potential applications (e.g., distillation desalination), which fit well into the discussion of the water−energy nexus at the global scale.[9−12] Starting from the initial demonstration of evaporation from a plasmonic nanoparticle (NP)−water suspension upon sunshine, a fundamental mechanism of such a phenomenon has been gradually unfolded, which changed the physical picture from the originally thought explosive evaporation (boiling)[7] to equilibrium evaporation.[13,14] A few years later, demonstration of SWE from Chen's group using light-absorbing carbon black and a thermal insulation design,[8] which showcased a high solar-to-vapor efficiency of 85%, excited extensive follow-up research in the materials and thermal engineering communities to invent new materials and design better thermal management schemes with the overarching goal of maximizing efficiency and enable applications like water desalination,[15] water sterilization,[6] wastewater treatment,[16] catalysis,[17] and energy generation.[18−20]

Like any other solar−thermal applications, SWE requires solar-absorbing materials to receive solar irradiation and convert it into heat. This heat is then transferred to water to

> Plasmonic nanoparticles can have strong light absorption around localized surface plasmon resonance peaks, which however lacks broad-band matching with the solar spectrum.

increase its temperature. Governed by thermodynamics, liquid water will always try to evaporate to saturate ambient air until the partial pressure of vapor in moist air is equal to the saturation pressure of water at a given temperature. Increasing the water temperature by solar heating will lead to higher saturation pressure, which will require an increase of water content (partial pressure) in air and thus promote evaporation. Because such evaporation is different from the much more explosive nucleate boiling, it is usually called equilibrium evaporation. Studies in this field mostly use low solar concentrations (<10 kW/m², i.e., 10 suns), and the resultant heat flux is not sufficiently large to enable nucleate boiling. A common metric for characterizing the SWE performance is the overall solar-to-vapor conversion efficiency, η_{s-v}, which can be written as

$$\eta_{s-v} = \frac{\dot{m}h_{LV}}{C_{opt}q_i} = \frac{Q_t}{C_{opt}q_i}\frac{\dot{m}h_{LV}}{Q_t} = \eta_{s-t}\eta_{t-v} \tag{1}$$

where $\dot{m}$ is the rate of mass evaporated per unit area from the solar absorber, h_{LV} is the total enthalpy of evaporation including sensible heat and liquid-to-vapor latent heat, C_{opt} is the optical concentration usually described by the number of suns, and q_i is the nominal direct solar irradiation, which is usually set to 1 kW/m^2 according to the AM 1.5G spectrum.[21] There are two major losses in the SWE process, from the solar-to-thermal conversion (η_{s-t}) and the thermal-to-vapor (η_{t-v}) conversion. The former highly depends on the light absorption efficiency of the solar absorber and the latter on the overall thermal management.

To help formulate this Review so that our discussed topics are relevant to the aspects of most interest to the research community, we first use text mining to analyze the abstracts of more than 100 journal papers published in the SWE field. Figure 1a shows the top 50 mostly repeated words in these
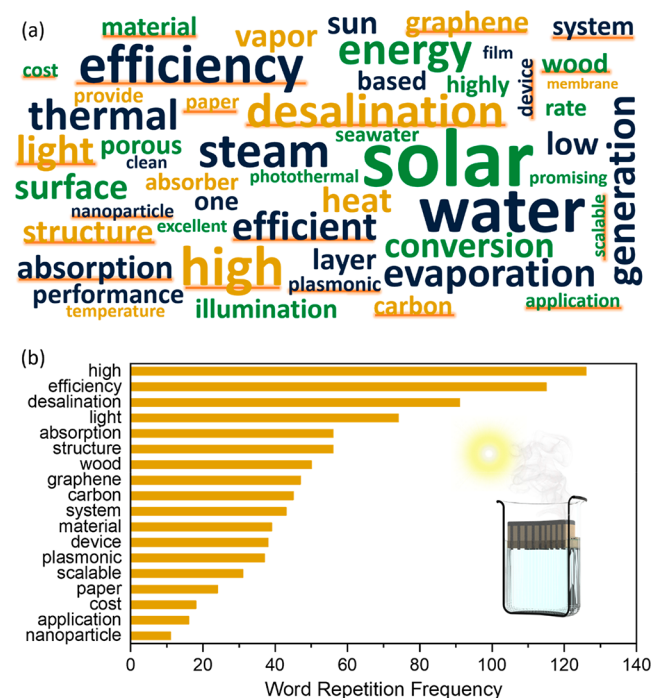

Figure 1. (a) Analytics of abstract text of papers in the SWE field from text mining. The abstracts of collected journal papers in the SWE field are turned into a corpus consisting of domain words relevant to SWE. The repetition frequency of each word appearing in the corpus is calculated, as illustrated by their corresponding font sizes in the word cloud. In the figure, the top 50 words ranked by their repetition frequencies are plotted. (b) Repetition rates of keywords that indicate the emphases of the SWE field, which are underlined in panel (a). Note: The abstracts analyzed were from the papers cited in this article.

abstracts, with the font sizes corresponding to their repetition rates. The repetition rates of selected keywords are also shown in Figure 1b. As can be seen, except those words directly from the name of the field (e.g., "solar", "thermal", "water", "evaporation", "steam", and "generation"), the text mining results show that this field intensively focuses on "material(s)", with the popular ones being "plasmonic" "nanoparticle(s)", "carbon", "graphene", "paper", and "wood" to reach efficient

"light" "absorption". Besides materials, "structure(s)", "system(s)", and "device(s)" are also studied extensively to either improve "efficiency" or enable different "applications", with "desalination" being the most investigated one. Because applications are the end goals of many studies, it is natural that "scalability" and "cost" are of concern to the researchers, but they seem to care much more about "high" "efficiency" as these are two of the most mentioned words.

Guided by the above analytics, we focus our discussion on materials engineering, system/structure/device design, and applications in the SWE field (Figure 2). After studying the
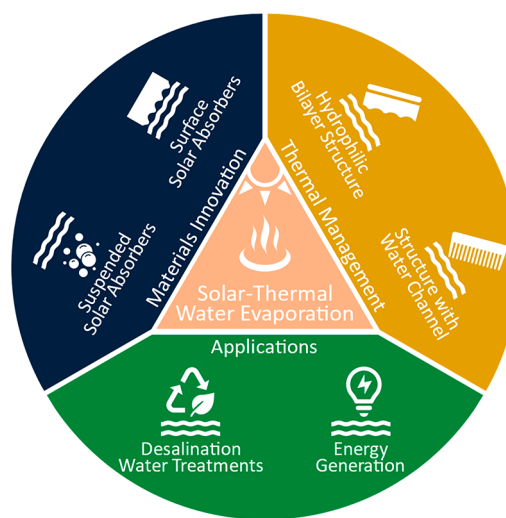

Figure 2. Schematic summary of the aspects covered in this article.

literature, we found that materials innovation are mostly related to improving the solar absorption to increase the solar-to-thermal conversion efficiency (η_{s-t}), although some are related to better water transport and thermal insulation. The system/structure/device design aspect in this field, however, mainly concerns improving the thermal-to-vapor conversion efficiency (η_{t-v}) by enabling better thermal management. Interesting yet simple applications, mostly related to water treatment of different kinds (e.g., desalination, sanitization, wastewater treatment) are the reasons why researchers with different backgrounds are drawn to this field. We also highlight some notable observations and innovative applications, which warrant continued research in our opinion. Finally, we present our outlook of the SWE field in the hope of providing useful suggestions to shape its future research directions and promote its further advancement. We would also like to refer readers to a few other Reviews on this field,[20,22−27] although their emphases or opinions might be different. Most of these Reviews appeared when we were preparing our own. The structure of this article is as follows: Materials Research for Solar Absorption; Thermal Management; Applications; Notable Innovations That May Promote Practical Applications of SWE; and Outlook.

Materials Research for Solar Absorption. Engineering solar-absorbing materials has been one of the most popular foci of the SWE field, with nanomaterials and low-cost materials being the two major themes. Depending on how the solar absorbers are placed with respect to water, they can be mainly categorized into two types, namely, dispersed absorbers (Figure 3a) and surface absorbers (Figure 3b). The former, mainly NPs, were initially studied as motivated by the
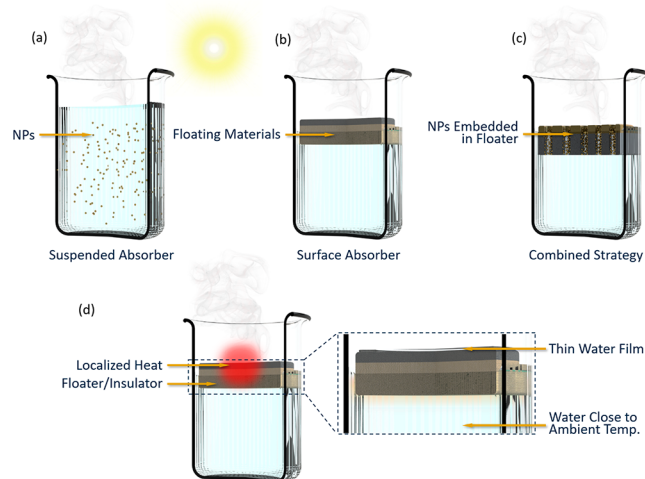
Figure 3. Different types of solar absorbers studied in the SWE field, including (a) suspended solar-absorbing NPs in water, which interact with solar light to generate heat and transfer it directly to the volume of water, (b) solar-absorbing materials floating on top of water, which usually wick water to the surface and heat up mostly the surface water, and (c) a strategy to enable plasmonic NPs also to be floating surface solar absorbers by embedding NPs into a porous floater. (d) Schematic of the SWE using a floating solar absorber and how such structures help localize heat in the absorber region.

interesting plasmonic light−NP interaction physics, while the latter were dominantly explored in order to achieve higher overall solar-to-vapor efficiency and potentially low-cost applications. The same kind of materials can be used in either of these two types of configurations, and their combinations have also been explored (Figure 3c). In this section, we review the materials research for both types of solar-absorbing strategies and the rationale behind these research activities, which is mainly to improve the optical absorption efficiency so as to enhance the solar-to-thermal conversion efficiency (η_{s-t}).

> Low solar concentration cannot provide high enough heat flux to trigger nucleate boiling, and thus, most solar−thermal steam generation is due to enhanced equilibrium evaporation at elevated water temperatures.

Optically Resistive NPs as Suspended Solar Absorbers. Optically resistive NPs have been explored for SWE as suspended solar absorbers. The most studied materials for such purposes are plasmonic NPs and carbon-based compounds, both of which have been picked up by the text mining analysis as high-repetition keywords (Figure 1).

Metallic NPs. Many metallic NPs can convert solar light into heat with a finite optical extinction constant. When the NPs are uniformly dispersed in water (sometimes referred to as "nanofluids") and subjected to sunshine, they can heat up the volume of water and thus promote evaporation. Representative works in this category can be found in refs 7, 14, and 28−35. Some noble metallic NPs (e.g., Au, Ag) can efficiently interact with light at certain wavelengths primarily due to the free electron oscillation and severe optical damping, i.e., localized surface plasmon resonance (LSPR) at the NP−water

interfaces. The LSPR strongly concentrates the electromagnetic field at the interfaces, leading to significant optical Joule heating in the NP. The size, shape, and composition of NPs can influence their optical extinction spectra, thus impacting the solar-to-thermal conversion efficiency (η_{s-t}). The simplest case would be spherical NPs. Neuman et al.[7] demonstrated the use of a spherical plasmonic NP suspension for SWE application, where they used a Fresnel lens to reach a solar concentration of 1000 suns and reported an overall solar-to-vapor efficiency of 24%. They believed that nucleate boiling was achieved but later realized it was equilibrium evaporation due to the fact that the solar concentration used in their experiments was significantly lower than the nanobubble generation threshold,[13] which should be in excess of 10^6 suns.[14]

However, metallic NPs usually have very sharp and narrow LSPR peaks, making them capable of utilizing only a small portion of the solar spectrum (Figure 4). For example, spherical Au NPs with diameters in the range of 9−100 nm have peaks in the 500−600 nm wavelength range with a full width at half-maximum (fwhm) < 200 nm.[36] Many attempts have been made to widen the extinction spectra of LSPR-supporting NPs, and interesting physics have been explored. The simplest route was to combine NPs of different sizes to use their varying LSPR peaks to broaden the overall suspension absorption spectrum, as practiced by the Halas group.[37,38] Engineering new NP structures is another route. For example, hollow Ag−Au alloy NPs were found to increase the fwhm of the optical extinction to 1000−1200 nm with a peak between 900 and 1300 nm (Figure 4).[29] Such hollow NPs not only covered a larger portion of the solar spectrum but also possessed higher absorption quality factors than scattering, thus increasing the solar-to-thermal conversion efficiency. The novel optical properties came from the unique hollow structures with random holes in the shell, which acted as irregular scattering centers to reduce coherent electron oscillations and promote Ohmic losses. A solar-to-vapor efficiency of 30% under 1 sun was reported at a NP concentration of 2.0×10^9 particle/mL, which was 40% higher than that of the spherical Au NP suspension with the same concentration. The authors also mentioned that the efficiency enhancement was also possibly due to the special geometry of the hollow NPs, which might have led to nanobubble nucleation in its interior. However, nanobubble nucleation requires a 10^6 solar concentration even for a NP excited by a monochromatic source at the LSPR peak.[14] It is also not clear why bubbles prefer to nucleate inside of the NP, which would lead to higher curvature and thus larger Laplace pressure that would actually impede nanobubble formation.[39,40] Another question is how the nanobubble inside of the hollow NP can rise to the surface and eventually release the vapor to the ambient. Bubbles with nanometer sizes should experience very small buoyancy, and coalescence into larger microsized bubbles is necessary to achieve efficient bubble ascending to the surface. All of these fundamental questions surrounding this nanoscale multiphase thermofluid phenomenon are yet to be answered and warrant further research.

In another study, polyhedron-shaped Ag NPs were shown to enable great tunability in bandwidth and peak position of the LSPR.[30] Polyhedron Ag NPs with a size of ∼80 nm could have absorbance spectra covering broad wavelengths of 350−1000 nm (Figure 4), which was attributed to the electric dipole and higher-order LSPR. With a concentration of 1.0×10^{13}
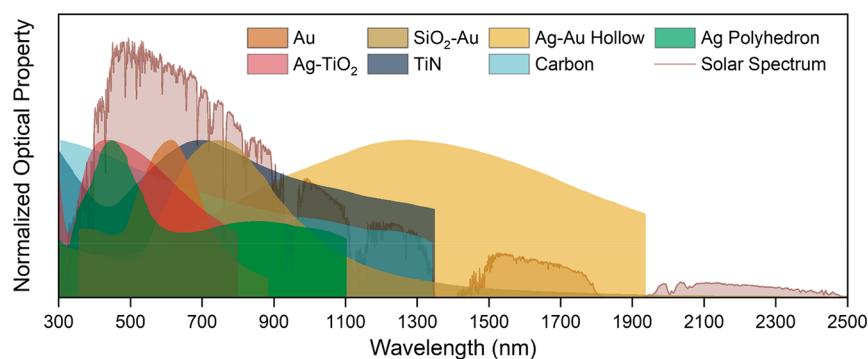
Figure 4. Optical absorptive bandwidth of representative NPs for SWE. For comparison, the normalized solar spectrum is also illustrated. Au:[36]; SiO$_2$−Au core−shell:[7]; Ag−Au hollow:[29]; Ag polyhedron:[30]; Ag−TiO$_2$:[31]; TiN:[32]; carbon:[32]. Note: the cutoff wavelengths of different NPs are due to the source data limitation.

particle/mL, the suspension of such NPs showed a solar-to-vapor efficiency of 82% at 1 sun. Due to the hybridization of LSPR of the Ag core and the TiO$_2$ shell,[41] Ag−TiO$_2$ core−shell NPs displayed improved optical absorbance spectra, achieving a fwhm of 350 nm at a LSPR peak of 430 nm (Figure 4).[31] However, the SWE performance of a suspension containing such NPs was inferior, achieving a solar-to-vapor efficiency of only 52% under 5 suns even at a high NP concentration of ∼1.9 × 10^{15} particle/mL. Besides noble metallic NPs, TiN NPs can also possess broad LSPR characteristics.[32] TiN has a complex dielectric constant, making it well-suited to achieve high absorption quality factors when it is made into NPs with a diameter of ∼100 nm. The optical absorbance spectrum of the TiN NPs showed a fwhm of ∼900 nm with a LSPR peak at 700 nm (Figure 4), which performed better than solid spherical Au NPs or carbon black NPs.[32] Its suspension showed a higher water-heating rate than the carbon black NP suspension with similar size and concentration.

> Because water evaporation rates in SWE devices are very low, water transport through floating solar absorption structures is not a bottleneck and does not need to be a primary design constraint.

Besides optical properties, NP suspensions also have different heat transfer patterns compared to surface solar absorbers. Given the large interface-to-volume ratio of the dispersed NPs in water, heat converted in NPs can rapidly transfer to water. The heating process depends on the solar intensity, optical extinction quality of individual NPs, their concentration, heat transfer across the NP−water interface, etc.[42] However, given the small thermal mass and relatively low concentrations of the NPs (10^9−10^{15} particle/mL), the local temperature due to non- or weakly concentrated solar irradiation is not high enough to result in bubble nucleation at the NP−water interface,[14,43] let alone that bubble nucleation around NPs has a higher threshold due to factors like Laplace pressure, interfacial heat transfer efficiency, and viscous dissipation effects.[39,40,44,45] It was analyzed that the local temperature around the NP needed to be above the spinodal temperature of water (∼550 K) in order to form nanobubbles.[46] Such a high temperature, however, cannot be reached by solar light with low optical concentrations. Nanobubble formation around NPs, mostly by coherent lasers,[13,46−48] is a very active research area in thermofluids,[39,40,44,45,47,49,50] and much still needs to be done to fully understand the physics. As such, a NP suspension under sunshine would heat water, and it was the elevated temperature that led to the observed enhanced evaporation at the water−air interface.[13,14]

Carbon-Based NPs. Carbon-based NPs are excellent solar absorbers for SWE applications[51] due to their high light absorption efficiency in the visible and near-infrared range (400−700 nm, Figure 4). They can also be much cheaper than their metallic counterparts. Ni et al.[14] studied carbon-based NPs suspended in water, including graphitized carbon black, carbon black, and graphene NPs. They found that in the steady state all three NPs with the same 0.23 vol % could reach a similar evaporation efficiency of ∼69% at 10 suns. However, the transient efficiencies were different, with the graphitized carbon black showing the highest evaporation efficiency and reaching the steady state the fastest. They concluded that the better transient performance of the graphitized carbon black was due to the smallest optical skin depth (∼1.8 × 10^{-6} m), a result of better dispersion due to the higher zeta potential (∼−40 mV). The smaller optical skin depth of the suspension localized the absorbed light and thus optical heating to a shallower region of water from the surface, and it also reduced natural convection of water. Both of these factors resulted in less water volume being heated, and thus, the temperature of water near the surface ramped up more quickly. These led to more efficient water evaporation in the transient state. However, in the steady state, the temperature of water is determined by the heat input (solar energy × η_{s-v}, where η_{s-v} is similar for the three tested carbon materials) and the heat loss to the environment (which determines the steady-state η_{t-v}). Because thermal insulation wraps were used for all three experiments, η_{t-v} should be similar, and thus, $\eta_{s-v} = \eta_{t-v}\eta_{s-t}$ turned out to be the same for all three materials. This is also easy to understand from the energy balance viewpoint: when the input heat is the same and the heat loss is the same, the neat energy added to the system (water) is balanced by the same amount of evaporation enthalpy taken away by the generated water vapor. In another study, Wang et al.[33] investigated SWE using carbon nanotubes (CNTs) dispersed in water, and the solar-to-vapor efficiency was expectedly found to increase with higher CNT concentration. This is apparently dominated by the change in η_{s-t}.

Carbon-based NPs were also mixed with other kinds of NPs to achieve additional functionalities in SWE applications. Reduced graphene oxide was used to decorate ferrimagnetic Fe_3O_4 NPs so that the composite magnetic NPs could be easily collected from water after solar evaporation for desalination purposes.[34] It was reported that an external magnetic field could successfully separate the NPs from the supersaturated brine. Another effort combined the graphene oxide nanosheets with homogeneous Au NPs,[35] but such a composite achieved a mere ~59% overall SWE efficiency at 16 suns, although it was 22% higher than that of the pure graphene oxide suspension. The authors mentioned that the Au NP could potentially reduce graphene oxide into graphene,[35] but the mechanism was not clear. It was indeed reported that the optical absorbance of reduced graphene oxide was better than that of graphene oxide,[52] and this might be the reason for the observed increase in SWE efficiency from the graphene oxide/Au NP composites.

Surface Solar Absorbers. In recent years, solar absorbers that float on the water surface have become more popular especially considering their better compatibility with thermal insulation designs and thus higher SWE efficiencies (Figure 3d). Such absorbers are usually structured to have density lower than that of water; therefore, they float. For such absorbers, they are usually soaked with a thin water layer, and as the materials receive sunlight, they heat up the soaking water and evaporate it at the water−air interface. Sometimes, the solar absorbers themselves are floaters, but in other cases, they are placed on top of a floater. The separate floater can bring in an additional benefit of thermal insulation because such materials are usually porous and have low thermal conductivity. Because the heat is largely localized in the solar absorber region (Figure 3d), the bulk water beneath the floater is not significantly heated up. This can reduce heat loss to the environment because the temperature difference between the bulk water and the ambient air, which are in contact with large surface areas, is smaller. Of course, an additional thermal insulation layer can be added to the surface of the container to further minimize heat loss.[8] Actually, the active solar-absorbing materials are not that different from those used in the suspended absorber scheme discussed in the last section.

> Compared to nanoparticle suspensions, surface solar absorbers are more popular due to their better compatibility with thermal insulation designs and higher solar evaporation efficiencies.

Metallic NPs. Metallic NP-based solar absorber materials have been used in floating absorbers, where the light-absorbing NPs are loaded into porous scaffolds.[53−59] The scaffolds can wick water to make contact with the solar -heated NPs (e.g., see Figure 3c). Instead of heating the bulk volume of water in the suspension case, water is primarily heated around the absorber-loaded region if the downward heat conduction to the bulk water is minimized. Because less water is being heated, the heated water can reach higher temperatures faster compared to the suspended absorber case, and thus, evaporation is usually more rapid. Also, because the bulk water is maintained at a lower temperature, its temperature difference with the ambient is smaller, and thus, less heat loss

to the environment is expected. However, this heat loss can be managed by thermal insulation around the container using low thermal conductivity materials like aerogel.[60−62] Additionally, compared to NP suspensions, NPs loaded into scaffolds can also avoid aggregation or loss of NPs during operation.

As in suspensions, plasmonic NPs in the scaffold can have strong optical absorption in a certain region of the solar spectrum due to the LSPR. Common NP materials for such absorbers include Au,[53,63] Ag,[64] Al,[65] Pt,[66] In,[67] and some metal oxides.[68,69] Loading metallic NPs into the scaffold has been exemplified by a number of studies from Zhu's group.[54,56,64] Chen et al.[56] deposited Au NPs on the surface of a nanofiber scaffold, and the solar-to-vapor conversion efficiency was as high as 83%. Zhou et al.[53] demonstrated that the optical absorption of Al NPs expanded to the wavelength of 2500 nm from 400 nm when the NPs were self-assembled in a highly porous anodic aluminum oxide (AAO) membrane. It was claimed that the tightly packed Al NPs inside of the membrane and their natural oxide shells coherently hybridized the LSPR modes to induce a red shift of the peaks and widen the fwhm. The porous AAO membrane also played an important role in enhancing light absorption by internally trapping light and reducing reflection losses. It led to an optical absorption of 96% in the solar spectrum and a solar-to-vapor efficiency up to 91% at 6 suns. This structure was shown to be capable of desalinating saline water to meet drinking standards. Zhou et al.[54] also showed that Au NPs could improve the optical absorptions when loaded into AAO membranes. Similar to the Al NP/AAO structure, the self-assembled and closely packed Au NPs in the porous channel of the AAO template were the main reason for the broad optical absorption across the photon wavelength of 400 nm−10 μm. This Au NP/AAO structure showed a solar-to-vapor efficiency of ~90% at 6 suns. In another study from Zhu's group,[64] Ag NPs were loaded to a porous template to form a structure functioning as both a pollutant detector and a steam generator with a solar-to-vapor efficiency of 80% under 4 suns. Liu et al.[70] loaded spherical- and nanorod-shaped Au NPs on a porous paper filter by casting a NP−water suspension. On the surface of the paper, the two kinds of Au NPs stuck together, and the contact points provided optical hot spots due to the coupled LSPR modes, which were not sensitive to the wavelength of the incident photon. It enabled 95% optical absorption over the broad wavelength range of 400−1400 nm. The Au NPs-deposited paper filter generated steam with an overall efficiency of 90% at 6 suns.

Some other notable studies in this direction are discussed briefly as follows. Zhang et al.[67] coated a microporous membrane with In NPs and achieved an efficiency of 84.2% for solar evaporation. Zhu et al.[66] loaded Pt NPs into a porous wood membrane and achieved an efficiency up to 85% under 10 suns. Both Ye et al.[68] and Wang et al.[59] used TiO_x in floating solar absorbers and achieved 50 and 82% solar-to-vapor efficiencies, respectively. The reason for the large difference in efficiency from these two works might be attributed to the different methods of assembling the NPs during the evaporator preparation process. In Ye's work, TiO_x NPs were coated sparsely onto the surface of a mesh,[35] but in Wang's work, the NPs were deposited to the cellulose membrane as a thick dense layer (5 um).[36] Kaur et al.[57] immobilized plasmonic TiN NPs in ceramic microfiber wools (CW). Compared to TiN NPs dispersed in water, the composite TiN NPs/CW film eliminated the absorption dips

observed in the NP suspension spectrum in the wavelength range of 300−600 nm, where a large portion of solar energy resides. The improvement was inferred from the LSPR hybridization of the aggregated TiN NPs in the CW membrane, and the device showed a solar-to-vapor efficiency of 80% at 1 sun. Chen et al.[63] loaded Au NPs into a poly(*p*-phenylene benzobisoxazole) nanofiber (PBONF) film, increasing the PBONF's optical absorption from 34 to 70% in the wavelength range of 400−2500 nm. At 1 sun, this structure was claimed to have a solar-to-vapor efficiency of 83%, which is somewhat puzzling given that the optical absorption efficiency was only up to 70%. It is possible that the optical properties were measured in the dry state and wetting the material might have led to a higher optical absorption efficiency. In comparison to other similar materials, the relatively low enhancement of optical absorption of the Au NPs inside of PBONFs is probably due to the isolated and uniformly deposited Au NPs, which prevented LSPR hybridization.

Carbon-Based Material. Typically used carbon-based materials for floating solar absorbers include carbon,[71] graphite,[72,73] carbon nanotubes,[74] graphene derivatives,[52,75−92] and carbonized biomaterials.[93,94] For example, Zhu et al.[71] reported a high solar-to-vapor efficiency of 90% under 1 sun using a carbon sponge, which had broad-band optical absorption and a cellular pore structure that could effectively wick water to replenish the evaporation region. Yin et al.[74] used a vertically aligned carbon nanotube (VACNT) array behaving similarly to a blackbody to reach a solar-to-vapor efficiency of 90%. The excellent evaporation performance was attributed to the strong optical absorption, as well as the ultrafast water transport through the VACNT layer due to the virtually frictionless wall of CNTs.[95−98] Hu et al.[76] and Fu et al.[82,86] prepared graphene oxide directly into an aerogel for the solar absorbers, which could self-float on water and wick water through the porous channels. Similarly, Chang et al.[99] synthesized 3D graphene oxide structures as floating solar absorbers.

Graphene derivatives have also been added to different structures for solar evaporation using printing,[100] drop casting,[101] vacuum filtration,[52,80,91,102] chemical binding,[92] or direct synthesis.[103] Li et al.[104] used wood as the floater with graphite sprayed on the surface for SWE and achieved a solar-to-vapor efficiency of 80% under 1 sun and 89% under 10 suns. They mentioned that, due to the anisotropic texture of wood, heat conduction in the cross-plane direction was reduced to minimize heat loss into the bulk water. With a thermal conductivity of 0.11 W/mK, it was not clear why the thermal insulation performance of the wood was claimed to be better than that of another thermal insulator (expanded polystyrene foam, EPF) with much lower thermal conductivity of 0.03 W/mK. Another feature emphasized in this wood-based solar absorber was the ability to efficiently transport water from the bottom to the solar-heated top surface due to the special cross-plane pits and spirals perpendicular to the wood surface.

Many other studies on SWE have also emphasized the ability to efficiently transport water to replenish evaporation.[74,94] Having efficient water transport channels can sometimes conflict with the notion of thermal insulation because water has thermal conductivity of ∼0.5 W/mK, higher than that of most porous floaters. It is then natural to limit the amount of water that is wicked into the porous floater as long as the evaporation region is sufficiently replenished. Actually, for SWE applications, water replenishment does not need to be a

primary design constrain because typical hydrophilic materials have much higher water transport capacity (~ 1000 kg/m²h)[104] than the solar evaporation rates (~ 1 kg/m²h). This fact allows one to limit the relative volume of water channels to ensure that the floater contains minimal amount of water, which can be realized by wisely engineering the floater structure. In the design by Ni et al.,[105] they opened a small number of narrow channels in a hydrophobic foam and filled the channels with water wicking materials to transport water below the floater to the solar absorber sitting on top of the floater, all realized with inexpensive off-the-shelf materials.

Some material/structure designs proposed in this field considered multiple factors that might influence real SWE applications. For example, besides the light absorption spectrum, the real-time changes in the sunlight direction can also impact SWE. In Ren et al.'s work, hierarchical graphene foam with continuous porosity was grown via plasma-enhanced chemical vapor deposition, which showed a dramatic enhancement in broad-band and omnidirectional absorption of sunlight, reaching an overall solar-to-vapor efficiency of 93.4%.[75] For similar purposes, Xu et al.[106] and Hong et al.[107] studied origami structures to maximize solar absorption during the whole daytime. The origami structures were also reported to benefit from multiple light reflections. Xu et al.[58] invented a Janus absorber consisting of two layers stacked in a vertical tandem geometry. The top was a hydrophobic layer with a highly porous poly(methyl methacrylate) (PMMA) structure coated with carbon black NPs as the solar absorber. The bottom side was a hydrophilic layer with porous polyacrylonitrile (PAN) films for wicking water. This structure allowed salt to be built only in the PAN films, which could prevent the blockage of the steam-escaping pathway in the top porous membrane. At 6 suns, this materials showed a solar-to-vapor efficiency of 83% with a continuous operation for 16 days without efficiency degradation.

> Inexpensive materials that are less prone to fouling will be more attractive in SWE applications.

Besides synthesized materials, there is also a large array of natural materials explored for SWE studies. Xu et al.[108] reported that natural and carbonized mushrooms could respectively achieve ∼62 and ∼78% solar-to-vapor efficiencies under 1 sun. Their capability of SWE was attributed to the unique natural structure of mushroom, i.e., umbrella-shaped black pileus, porous texture, and fibrous stipe with a small cross section, which naturally helped solar collection, water transport, and thermal insulation. Lin et al.[109] also reported that carbonized kelp, which displayed high solar absorption, a porous microstructure, and a hydrophilic surface, could enable highly efficient SWE (84.8% under 1 sun) and seawater desalination. Similarly, other carbonized plants like lotus,[94,110] daikon,[111] and sugar cane[112] were found capable of SWE. Han et al.[113] used a carbonized eggshell membrane for SWE, which was found to have a porous microstructure that enabled efficient water/vapor transport and localized heating, and a solar-to-vapor efficiency greater than 75.6% was achieved. In additional to carbonizing natural materials, Chen et al.[114] demonstrated a self-floating carbonized facial tissue for SWE, reporting a 95% solar-to-vapor efficiency under 3 suns. While these materials are attractive due to their potential low cost

and the notion of waste reuse, carbonizing them does still need energy, which does not necessarily make them "free." In real water treatment applications, how to prevent these materials from fouling, especially biofouling, may still present a great challenge.

Discussion and Perspective. As discussed in this section, materials innovation has been a major component in SWE research, with a primary objective to enhance light absorption efficiency (i.e., to increase η_{s-t}) with some concern for water transport and heat loss. Overall, we can conclude that for practical SWE applications floating solar absorbers are likely superior to their suspension counterparts, mainly due to thermal and materials management (e.g., material reuse) concerns. In addition, floating structures allow more flexible modular design to optimize SWE, such as loading different solar-absorbing materials and the use of simple engineering designs (e.g., water wicking channels in thermal insulating floaters)[105] to minimize heat loss. We are excited to see innovative materials possessing high solar absorption efficiencies, but they can be expensive (e.g., metallic NPs, CNT, and MXene[115]) or difficult to fabricate or have practical concerns in real applications, with the last factor applicable to any materials used for SWE application to different extents. Carbonized natural materials are emerging for SWE applications due to their wide availability and potential low cost. However, for real application, preventing material fouling to maintain the longevity of any solar absorbers used in SWE will be critical. We believe much knowledge should be learned from the already mature water treatment community (e.g., pretreatment membranes). We have also seen the use of inexpensive yet light-absorbing materials, like carbon black, stained paper,[16] or cermet coating,[105] to achieve high solar-to-vapor conversion efficiencies. These cost-effective materials may help lower the barriers in translating laboratory prototypes to real applications.

> ## Carbonized natural materials find popularity in solar–thermal water evaporation studies.

Thermal Management. Although briefly touched in the last section and the fact that it almost always go hand-in-hand with solar absorber studies, we discuss thermal management as a separate topic because we believe that better thermal design is as important as, if not more important than, materials development for solar absorbers. Better thermal management can largely prevent heat loss to the environment so that more collected solar energy is directed to evaporate water, increasing the thermal-to-vapor efficiency, η_{t-v}. Before discussing studies on thermal management, we would like to discuss what should really be counted as losses in SWE. There are two scenarios (Figure 5a,b): (1) a floating SWE device is directly placed in open water, as demonstrated in ref 15, and (2) SWE of water in a container, which applies to more applications like rooftop devices. The latter is likely more practical because pretreatment of water can be more easily integrated. In the first scenario, heat leakage from the absorber to water underneath of the floater should be considered as loss because this is heat lost to the environmental water as a heat sink. In the second scenario, however, heat transfer from the absorber region to water underneath of the floater may not be considered a major loss if the container is properly insulated from the environ-

ment. This is because water in the container will eventually be evaporated and its temperature increase due to heat leaked from the absorber contributes to the total evaporation enthalpy. This point can be proven by the work from Ni et al.,[14] who used various carbon materials suspensions with different heating skin depths and showed that the steady-state solar-to-vapor efficiency was not a function of heating skin depths. In most SWE studies, especially those in recent years using floating solar absorber structures, thermal management structures can be generally classified into two types: hydrophilic bilayer structure (Figure 5c) and structure with dedicated water transport channels (Figure 5d).

> ## A hydrophobic thermal insulator with dedicated water transport channels is a better option for thermal management.

Hydrophilic Bilayer Structure. The bilayer thermal structure is generally composed of two layers with distinct functions, with the top layer for solar absorption and the bottom layer for thermal insulation, water transport, and floating. In the original work by Ghasemi et al.,[8] a bilayer structure consisting of a carbon foam floater supporting an exfoliated graphite layer as the solar absorber with 97% solar absorption efficiency was employed. The carbon foam, which has low thermal conductivity due to its porosity, was meant to provide thermal insulation to minimize heat leakage from the solar absorber to bulk water in the container. In the meantime, to ensure water supply to replenish evaporation, both layers were made hydrophilic. A solar-to-vapor efficiency up to 85% was reported at 10 suns. However, the hydrophilic carbon foam would be soaked with water during operation, and its thermal conductivity would be close to that of water, much higher than that of its dry state. Many follow-up studies have used similar bilayer structures with a variety of solar-absorbing materials and foams,[116] papers,[117] and woods[73,101,117–121] as the supporting layer for thermal insulation and water transport.

> ## Only heat not eventually used towards water evaporation should be counted as loss.

Structure with Dedicated Water Transport Channel. Instead of using the whole floating materials to wick water, which would actually impair thermal localization, as mentioned in the Surface Solar Absorbers section, some researchers implemented independent wicks in a nonwetting floater to minimize heat leakage through water while providing sufficient water supply to the evaporator. This was exemplified by the designs from Ni et al.,[15,105] where an insulation foam limited the heat conduction to the water underneath, but several fabric wicks embedded in the foam were used to transport water through the foam to the evaporation surface (Figure 5d). Similarly, Guo et al.[80] used a structure including separate capillary tubes through a thermal insulator to reduce heat loss. Li et al.[81] fabricated a jellyfish-like structure with a porous carbon black/graphene oxide composite layer for solar absorption and EPF for thermal insulation, while graphene oxide pillars were used for water transport. Other materials used to function as water transport channels include graphene oxide with 2D water paths,[102] graphene oxide/nanofibrillated cellulose,[100] cellulose
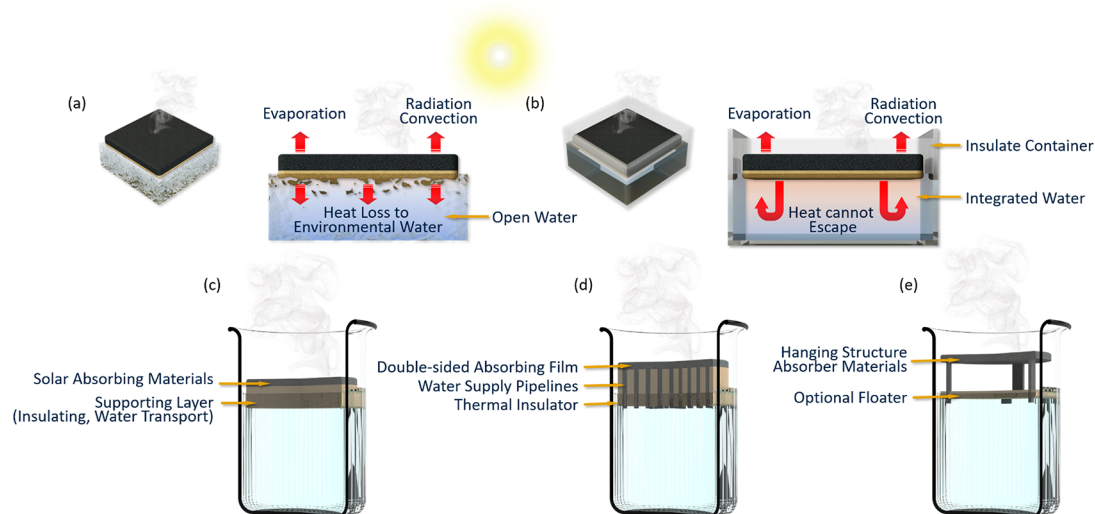
Figure 5. Schematics of (a) a SWE device floating in open water where heat conduction from the heated solar absorber region to water beneath the floater should be counted as loss, and (b) a SWE device placed in a container that is insulated from the environment. In (b), heat transfer from the solar absorption region to water below the floater contributes to heating water that is eventually evaporated, and thus, it should not be counted toward loss. (c) Hydrophilic bilayer structure with the supporting layer working as both a floater and a water wick, (d) structure with dedicated water transport channels, where the floater is hydrophobic but with water wicks embedded for water transport, and (e) hanging structure using the air gap for thermal insulation.

wrap,[100] air-laid paper,[16] carbon black/polyacrylonitrile nanofiber,[122] porous filter paper,[123] and polyurethane sponge.[124] Advanced manufacturing techniques have also been implemented to produce some of the structures with independent water transport channels, such as self-assembly,[53] 3D printing,[100] femtosecond laser processing,[124] and flame treatment.[125] However, we have not seen systematically better SWE performance from devices using sophisticated materials or manufacturing techniques than those used simple fiber wicks or wraps.[15,105,123]

Recently, some studies used hanging structures that could leverage both sides of the solar absorber for evaporation (Figure 5e). Such structures wicked water from the water container via narrow channels connected to the sides of the solar absorber, and the air gap between the absorber and the water surface worked as the thermal insulator. Liu et al.[126] showed that this structure could prevent heat dissipation to bulk water and enable double-sided evaporation upon solar irradiation, achieving a solar-to-vapor efficiency of 89.9% at 1 sun. Peng et al.[127] used a similar structure, which was found to enhance evaporation due to a larger evaporation area from both sides of the solar absorber. When compared to a conventional structure, they showed that the hanging structure had a 14% higher efficiency, reaching a value of 87% at 1 sun. Yu et al.[128] studied similar structures and achieved a solar-to-vapor efficiency of 98.1%. They attributed the high SWE performance to easy vapor escaping from the hanging structure, lower evaporator temperature that reduce the driving force for heat leakage to ambient, and negligible convection loss and radiation loss from the evaporator. We note that, while air has very low thermal conductivity (0.02 W/mK), the heat transfer mode through air would mainly be convection. In open water, forced convection due to wind can quickly cool the solar absorber. When used in a container configuration, natural convection may still play an important role in heat transfer. Aside from thermal management, the backside of the hanging absorber can provide an additional evaporation area. It will at least enhance the dark condition evaporation rate given

the larger surface area, but reflected light from ambient may also be absorbed by the backside of the evaporator, which can contribute to increasing the total evaporation rate.

Thermal Insulation Materials. Besides designing appropriate thermal insulation structures, there have also been extensive materials development activities for both of the above thermal insulation strategies. To serve as an ideal thermal insulating layer, materials with low thermal conductivity are generally used, including wood,[101,104,121,129−132] paper,[117,123,133] aerogel,[120,124,134−136] polystyrene (PS) foam,[15,81,90,102,105,111,137−142] expanded polyethylene (EPE) foam,[16,80,115,125,143,144] and other materials.[84,100,116,122,145−151]

Wood has been a popular material explored in SWE studies. Liu et al.[101] reported that the inherent physical and chemical properties of wood such as high porosity, light weight, low thermal conductivity, and hydrophilicity made it an excellent candidate for SWE applications when it is combined with graphene oxide for solar absorption. However, as mentioned earlier, hydrophilic wood would be soaked with water in operation, making heat transfer from the solar absorber layer to bulk water more efficient. The authors measured the thermal conductivity of hydrated wood to be 0.525 W/mK, which is much larger than that of dry wood. Jia et al.[130] used different natural wood (e.g., poplar, pine, and cocobolo) as the thermal insulating layer and found that poplar wood with a thermal conductivity of 0.27 W/mK in the dry state exhibited the highest solar-to-vapor efficiency. They attributed this to the minimized heat transfer from its carbonized top layer to the bulk water. Liu et al.[132] demonstrated an artificial tree structure with a reverse-tree design and carbonized the tree surface for solar absorption. Due to the anisotropic thermal conductivity of natural wood, the prepared structure displayed low thermal conductivity of 0.11 W/mK. It was claimed that the nature-made 3D interconnected channel pores enabled efficient water transport, while the heat transfer was also effectively blocked between layered channels. Li et al.[104] used wood as the floater with graphite sprayed on the surface. They also mentioned that due to the anisotropic texture of wood, heat conduction in the
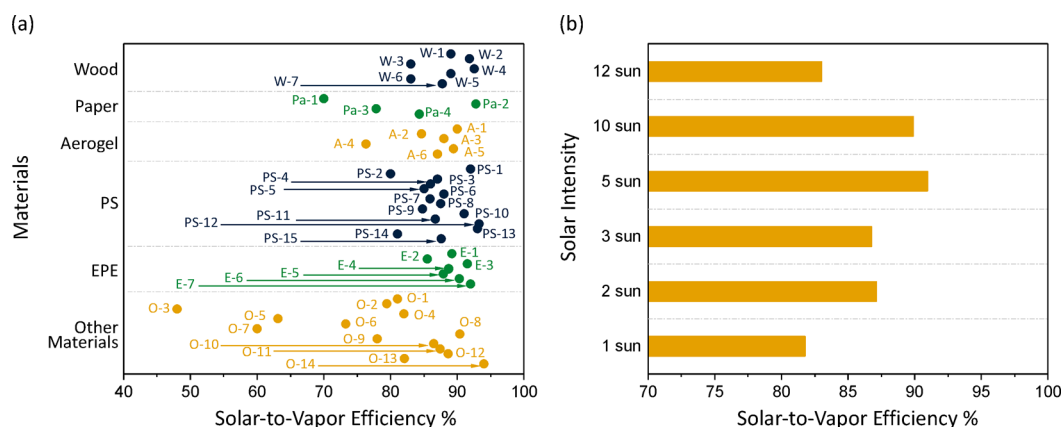
Figure 6. (a) Reported overall solar-to-vapor efficiency values from the literature for different thermal insulating materials. (b) Solar-to-vapor efficiency for different solar concentrations, where data are averaged from different reports. References in panel (a) are W(ood)-1:[132]; W-2:[131]; W-3:[101]; W-4:[121]; W-5:[104]; W-6:[153]; W-7:[154]; Pa(per)-1:[133]; Pa-2:[155]; Pa-3:[156]; Pa-4:[157]; A(erogel)-1:[124]; A-2:[136]; A-3:[120]; A-4:[135]; A-5:[134]; A-6:[158]; PS (polystyrene foam)-1:[90]; PS-2:[102]; PS-3:[141]; PS-4:[140]; PS-5:[139]; PS-6:[138]; PS-7:[111]; PS-8:[81]; PS-9:[109]; PS-10:[159]; PS-11:[160]; PS-12:[161]; PS-13:[162]; PS-14:[163]; PS-15:[164]; E(PE)-1:[80]; E-2:[16]; E-3:[144]; E-4:[115]; E-5:[125]; E-6:[165]; E-7:[166]; O(ther materials)-1:[151]; O-2:[150]; O-3:[149]; O-4:[122]; O-5:[147]; O-6:[146]; O-7:[84]; O-8:[116]; O-9:[167]; O-10:[110]; O-11:[168]; O-12:[169]; O-13:[80]; O-14:[170].

cross-plane direction was reduced to minimize heat loss into the bulk water.

Paper is another material extensively studied as thermal insulators because of its low cost, low thermal conductivity, and interconnected porous structure. Liu et al.[133] presented a bilayer structure for SWE by daubing carbon particles on paper. They claimed that the paper worked as a thermal insulator to hinder heat loss to bulk water, and its thermal conductivity in the wet state was found to be 0.44 W/mK. Through an optimization study, a thickness of nine-layer papers was found to be optimum for SWE due to the appropriate thermal resistance and water permeability. Chen et al.[123] deposited Ag nanostructures on a filter paper by vacuum filtration and claimed that the filter paper could serve as a thermal insulator to prevent heat transfer from the Ag solar absorber to bulk water.

Aerogels are also popular for thermal insulation in SWE studies due to their low thermal conductivity. Jiang et al.[135] designed a bilayer aerogel structure consisting of hydrophilic cellulose nanofibrils (CNFs) as building blocks and CNT layers for solar absorption. It was claimed that the ultralow density CNF reduced the parasitic thermal loss to the bulk water due to its high porosity, which also provided efficient water transport. Mu et al.[120] reported a hydrophilic conjugated microporous polymer (CMP) aerogel-based device using 1,3,5-triethynylbenzene, 1,4-dibromobenzene, and 1,4′-dibromobiphenyl as building blocks. Due to its high porosity of more than 94%, the CMP displayed dry state low thermal conductivity of 0.022 W/mK. Qin et al.[134] used a hydrophilic ultralong hydroxyapatite (HAP) nanowire aerogel for thermal insulation as well as water transport and a hydrophobic CNT as the evaporator to construct a SWE device in a bilayer structure. Owing to the low thermal conductivity of the HAP nanowire aerogel, the heat localization was claimed to be optimized. Yin et al.[124] assembled a device with a Ti foam, aerogel cotton, and polyurethane sponge for SWE. In this integrated evaporator, the treated Ti foam had broad-band solar absorption of efficiency higher than 97%, and the aerogel insulation cotton acted as a thermal insulator to suppress the heat transfer to the bulk water. However, the above-reported superior thermal insulation materials were based on dry state

thermal conductivity, and when soaked with water in operation due to their hydrophilicity, the insulation layers would possess thermal conductivity close to that of water (~0.55 W/mK), roughly equivalent to having no thermal insulation. Another concern is that aerogels are brittle, which might complicate manufacturing and field operation.

PS and EPE foams are also attractive as the insulation layer in SWE devices due to their extremely low thermal conductivity and low cost. Unlike hydrophilic materials (e.g., wood and paper), PS and EPE foams cannot transport water due to their hydrophobic feature. Therefore, wicks or other independent water channels are needed to transport water to the evaporation surface. Ni et al.[105] constructed a SWE device using commercially available cermet-coated copper as the solar absorber and a PS foam with a thermal conductivity of 0.03 W/mK as the floater and thermal insulator. In their device, a fabric wick passed through the foam to transport water from the container to the solar absorber surface to replenish the evaporation. Similarly, Guo et al.[80] used a thermal insulator made of EPE foam to break off the direct contact between the solar-absorbing layer and bulk water and installed water supply pipelines for water transport. Peng et al.[152] used EPE foam covered by linen cloth as a water wick for thermal insulation in SWE. Li et al.[81] reported a jellyfish-like device using a EPS matrix with thermal conductivity of 0.03 W/mK in the dry state as the thermal insulating layer. Vertical graphene oxide pillars were added by 3D printing for water transport. The thermal conductivity of the whole evaporator was estimated to be ~0.08 W/mK in the wet state. Zhu et al.[111] utilized carbonized daikon as the solar absorber and a 1 cm thick PS foam as the thermal insulator wrapped with cotton gauze for water transport. The gauze-wrapped PS foam exhibited low thermal conductivity of 0.049 W/mK. Yin et al.[144] used a porous double-network hydrogel (p-PEGDA−PANi) as a broad-band solar absorber integrated with an EPE foam for thermal insulation. The foam was wrapped by cellulose for water supply. Deng et al.[16] used ink-stained paper for solar absorption and an EPE foam for thermal insulation. The air-laid paper also served as a water wick to transport water to the evaporation surface. Zhao et al.[115] developed a 3D MXene architecture supported by an EPE foam acting as a thermal
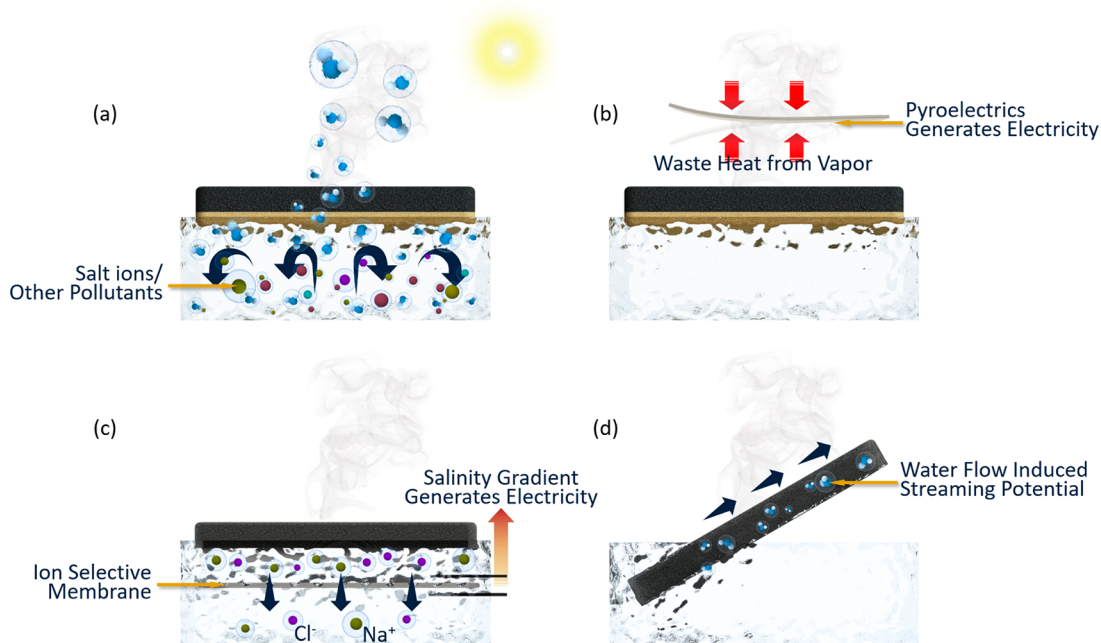
Figure 7. Schematics of representative applications explored using SWE: (a) water desalination/treatment; (b) energy generation using pyroelectric and piezoelectric effects; (c) energy generation utilizing a salinity gradient-induced osmotic potential; and (d) energy generation using a steaming potential.

insulation layer, and a hydrophilic wrap around the foam was implemented for wicking water.

Many other materials have also been used as the thermal insulating layer in SWE devices, such as porous carbonized lotus seedpods,[110] sugar cane stems,[123] silicone,[151] polyvinylidene fluoride (PVDF),[122] melamine foam,[116] PDMS foam,[148] and polyurethane sponge.[146] However, almost all of these thermal insulating materials have thermal conductivity larger than that of standard thermal insulators like the EPE foam (thermal conductivity of 0.03 W/mK). Like done by Ni et al.[105] and a number of other designs discussed above, utilizing the low thermal conductivity of hydrophobic EPE or PS foams but implementing limited water transport pathways is likely the most effective and low-cost strategy for thermal insulation in SWE applications. In Figure 6a, we summarize the reported solar-to-vapor efficiencies from the literature using different thermal insulating materials. While these efficiencies are convoluted by the performance of solar absorbers (η_{s-t}), we do see that PS and EPE foams enabled efficiencies higher than 85%, except from two studies. This may be attributed to their low thermal conductivity and nonwetting characteristics, which lead to high η_{t-v}.

Discussion and Perspective. After the above discussion, we would like to revisit the real benefit of thermal insulation. For SWE devices to operate in open water, a thermal insulation layer is essential because it can effectively prevent excessive heat loss from the heated solar absorber layer to the environment. This will lead to higher overall solar-to-vapor efficiency. For the SWE devices sitting in a container, heat localization within the solar absorber layer can help increase the evaporation temperature and thus evaporation rate. If we assume a constant humidity in the ambient air and a feedwater temperature of 25 °C, the amount of energy needed to saturate the air (ΔE) with water vapor at a given elevated temperature (T) around the heated solar absorber is

$$\Delta E = \Delta m(c(T - 25) + \Delta h(T)) \tag{2}$$

where c is the specific heat of liquid water, which is almost a constant = 4.18 kJ/kg-K at the temperature range of interest (20−100 °C). Δm is the mass of evaporated water. Δh is the enthalpy of vaporization at the temperature of water in contact with air. It is noted that Δh decreases as temperature increases (e.g., Δh = 2454.12 kJ/kg at 25 °C and 2257.03 kJ/kg at 100 °C). However, due to the need for sensible heat to heat water from the initial 25 °C to the elevated temperature, the total ΔE increases with temperature slightly (e.g., ΔE = 2454.12 kJ/kg at 25 °C and 2570.53 kJ/kg at 100 °C).[171] As a result, from a pure thermodynamic point of view, localizing heat within the solar absorber region, which maintains surface water at a higher temperature, does not necessarily increase the thermal-to-vapor efficiency. We do see many studies showing that heat localization in the solar absorber region helps increase the overall solar-to-vapor conversion efficiency. This is likely due to the heat leakage to the environment through the container walls. Without heat localization, the water temperature in the container will be higher, and due to the large contact area with the ambient, heat loss is enlarged if the walls are not well-insulated. A quantitative evaluation comparing different thermal management strategies (e.g., wall insulation and heat localization) for SWE in a container is needed. The above discussion is assuming a steady state. In the transient state, heat localization can lead to faster ramping up of evaporation rates, which might be important for SWE applications due to weather conditions influencing solar intensity. In a similar sense, increasing the solar concentration, which increases the absorber temperature, should not increase the energy efficiency at the steady state either, but it can apparently increase evaporation rates due to higher energy input. The usually observed higher solar-to-vapor efficiencies at higher solar concentrations (Figure 6b) cannot be properly explained by the thermodynamic energy balance and may be due to other factors like transient heat leakage to the environment.

Besides thermal insulators, water transport is usually emphasized to ensure efficient replenishment of evaporation in the solar absorber region. As a result, many studies engineered materials that are hydrophilic to wick water, which is not beneficial for heat localization due to the relatively high thermal conductivity of water. We need to evaluate how necessary it is to make the whole floating layer hydrophilic for water transport. If we consider 1 sun, the maximum evaporation rate would be ~1.43 kg/m²h. This is already slightly lower than the wicking flow rate (1.87 kg/m²h) of hydrophobic porous materials[172] and is 3 orders of magnitude smaller than the transport-limited flow rates in typical hydrophilic porous materials, which are above 1000 kg/m²h.[104] As such, water transport should not be a barrier given the low evaporation rates, and using nonwetting foam materials with limited wicks (occupying <0.14% of the surface area) can cost-effectively manage water transport while maximizing heat localization. It is our opinion that the thermal insulation materials used for SWE should be developed with the aim of reducing cost, improving durability, and ensuring easy manufacturing, and polymer foams satisfy all of these requirements.

Applications. It is clear that the rapid expansion of research in SWE is largely motivated by its attractive potential applications of using renewable solar energy for water treatments. Other applications, mostly complementary to the water treatment capability in the same device, have also been proposed. These are reviewed in this section.

Desalination and Water Treatments. SWE is naturally attractive for distillation water desalination (Figure 7a) as it uses otherwise wasted low-grade solar energy and should principally work well as distillation desalination techniques (e.g., multistage flash, multieffect flash) have historically produced high-quality water with ion removal efficiency even higher than that of the more popular reserve osmosis methods.[173] While providing clean water for household use (~300 L per person) with SWE devices is impractical, the water production rate of SWE, although low, may still make sense if only drinking water needs to be supplied. In an ideal scenario (8 h of 1 kW/m² full sunshine daily and 100% solar-to-vapor efficiency), the daily water production rate is ~11.5 L/m² of SWE surface at 1 sun. If we consider that an adult daily water intake is ~3.7 L,[174] a 1 m² SWE device can be sufficient for a family of three. However, in a practical experiments by Ni et al.,[15] the daily fresh water production rate was only 2.5 L per m², which showed that much engineering work would still be needed to improve system performance in real-world applications.

There have been a larger number of reports pertinent to water desalination using different SWE designs, involving materials like graphite films,[72] graphene oxide-coated wood,[101,131] graphene/metal/polymer composite membranes,[92,175] microporous membranes with NPs,[67,176,177] carbon ink-stained paper,[16] flame-treated foam,[125] and a bilayer Janus membrane.[178] Salinity has been used as a metric to evaluate the performance of SWE desalination devices. Almost all relevant reports[58,67,72,81,131,179] demonstrated the reduction of salinity to meet thresholds for drinking water (500 ppm) set by the World Health Organization and the U.S. Environmental Protection Agency.[180] This is not surprising because thermal distillation (e.g., multistage flash) has always been able to reach high salt removal rates of >98%.[173] There have also been desalination demonstrations of real saline water.

For example, Li et al.[102] used their graphene oxide-based SWE device and successfully desalinated water from the North Sea (salinity 1.4%) and Red Sea (salinity 4.1%). Li et al.[81] also demonstrated the desalination of seawater from the Dead Sea and Chesapeake Bay.

Similarly, SWE can also be used for other distillation-enabled water treatment, such as heavy metal removal,[181] pollutant removal,[31,34,64,90,182−185] sludge drying,[94] oil spill cleaning,[186] and water sterilization.[6]

Energy Generation. Energy generation from effects of SWE has also been explored by a number of studies. Zhu et al.[71] reported that a ferroelectric fluoropolymer, polyvinylidene fluoride, could be introduced to a SWE system to harvest the thermomechanical responses from the generated water vapor based on the coupling of the pyroelectric and piezoelectric effects, demonstrating a SWE-induced electrical potential (Figure 7b). The highest output power was calculated to be 240 μW/m², corresponding to a solar-to-electricity efficiency of 2.4×10^{-5}%. Zhu et al.[19] used a PDMS sponge coated with CNT/cellulose nanocrystals for broad-band solar absorption. Meanwhile, due to heat localization, a temperature difference was generated between the sponge and bulk water, which allowed a thermoelectric module to generate electricity via the Seebeck effect. The largest electrical power density achieved was 6.73 W/m² under 5 suns, which translates to a solar-to-electricity efficiency of 0.13%. Yang et al.[187] reported that the evaporation-induced salinity difference could also be used for electricity generation (Figure 7c). In his study, a hybrid device with a top layer of CNT-modified paper and a bottom layer of an ion-selective membrane was made floating on seawater. Due to evaporation, a salinity gradient was created from the evaporator to the bulk seawater, which in turn drove the directional transport of salt ions—a mechanism that has been explored for harvesting osmotic potentials from salinity gradients.[188−191] Such an osmotic electricity generation produced a power density of 1 W/m², corresponding to a solar-to-electricity efficiency of 0.1%. Ding et al.[192] reported that the liquid flow within the porous structure of SWE could result in a streaming potential, so that natural water evaporation from the surface of the nanostructured carbon coating could generate electricity (Figure 7d). There are also demonstrations of using SWE to produce energy for other applications like hydrogen production,[193] photothermal catalytic reaction,[17,193] triboelectric generation,[194] and bioethanol production.[195]

Discussion and Perspective. However, barriers for the wide adoption of SWE devices for water treatment still exist. First is how to compete with the state-of-the-art. Ni et al.[15] estimated the cost of their SWE device ($1.5/m³) and compared it to conventional solar stills ($15/m³) and reverse osmosis with the same scale ($5−10/m³), showing that the SWE evaporator could be economically competitive for desalination compared to existing technologies. However, they included only the materials cost of the SWE system itself without taking into account peripherals (e.g., pretreatment), which can be essential for the longevity of such systems. In a recent review on solar−thermal desalination,[23] Wang et al. mentioned that SWE-based desalination, even with latent heat reuse, would be far less energetically efficient than reverse osmosis desalination, which has been seen powered by solar photovoltaics,[196,197] due to the inherent energy requirement for overcoming the latent heat in SWE. They, however, mentioned that SWE could have niche applications for high-salinity water desalination where reserve
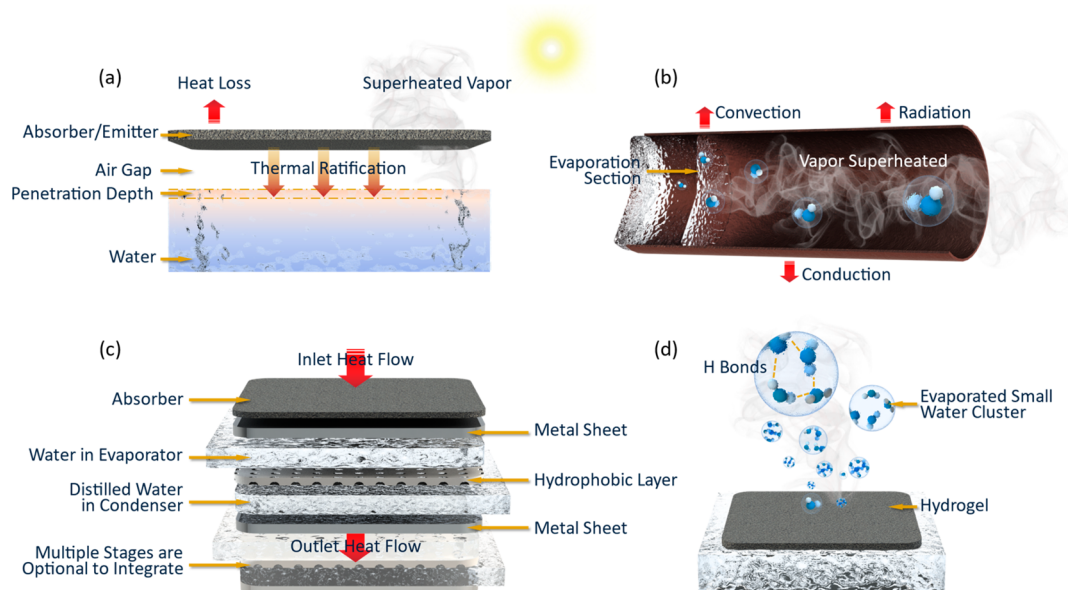
Figure 8. Schematics of (a) superheated vapor generation using thermal concentration and radiation; (b) superheated vapor generation using continued heating of the vapor phase; (c) condensation heat reuse leveraging a cascade membrane distillation design; (d) claimed reduction of water evaporation enthalpy due to a special hydrogel enabling water evaporation as clusters instead of individual molecules.

osmosis is currently facing technical challenges. We would like to mention that a large number of factors can influence the eventual cost of SWE desalination such as peripherals, maintenance, and durability. Durability can be a critical barrier for SWE technology transfer. Although there were a few studies demonstrating that SWE devices could work for many cycles[16,58,78,88,175,179] and some with self-salt cleaning ability by redissolving condensed salt back into water during nighttime,[15] biofouling may be a much greater challenge to mitigate and can degrade desalination devices in the long term. Even in the most sophisticated reverse osmosis and thermal distillation desalination plants, stringent pretreatments involving multistages of filtration and chemical treatment are needed,[198,199] yet membrane replacement is still required periodically, costing millions of dollars. Most of the SWE devices were proposed for niche applications in remote and underdeveloped areas, where centralized infrastructures are lacking, making water treatment using free solar energy attractive. However, in these areas, pretreatment can be difficult and costly, but without it, the SWE devices may foul quickly. There are also other practical difficulties in SWE operation, such as the inconsistency of sunshine, condensate reducing the solar intensity reaching the solar absorber, and the need to track the sun direction for maximal solar energy collection. These, however, are less critical and can be resolved using proper engineering designs (e.g., using a fan to blow away vapor[169] and using origami structures[106,107] to maximize solar absorption during the whole day).

For SWE-enabled energy generation, we notice that the efficiencies of power generation based on SWE were extremely low (<0.13%) and so were the power densities. For example, in Yang's work,[187] the generated electrical power was up to 1 W/m^2, and it was 240.7 μW/m^2 from Zhu's work.[71] It was proposed that such generated power might be sufficient to drive low-power electronics such as sensors,[200] but the extremely low efficiency and bulkier footprint make them impossible to compete with solar photovoltaics, which have some commercial products possessing efficiencies higher than

20%. However, it is possible that such power can be used to drive peripherals, such as a fan for vapor transport or a motor to direct the solar absorber surface to always face the sun. We have to note that combining SWE with power generation requires additional components, such as thermoelectric modules[19] and ion-selective membranes,[187] which will inevitably increase the system cost. It would be more efficient and cost-effective to cut out a small area in the SWE solar absorber to install a photovoltaic panel for power generation if power is needed.

It is our belief that currently it is very difficult for SWE to compete with state-of-the-art water treatment technologies, such reverse osmosis and thermal distillation, in terms of maturity, cost, and throughput, and SWE-based energy generation would be even so. It will also face competition from other emerging technologies that can potentially leverage nonconcentrating solar heating for desalination, such as directional solvent extraction,[201−205] membrane distillation,[206,207] and forward osmosis.[208,209] However, there can still be niche applications like desalination of high-salinity water, water supply, and sanitization in remote and underdeveloped areas if technical barriers can be overcome.

Notable Innovation and Findings That May Promote Practical Applications of SWE. After reviewing a large number of studies in the SWE field, we would like to use this section to highlight some notable innovations that can potentially improve or broaden the future applications of SWE devices. We also discuss an interesting finding claiming significantly reduced latent heat of water evaporation in a hydrogel as it is fundamentally intriguing and can potentially impact fields beyond SWE, if it is proven true.

Superheated Vapor Generation. The first innovation worth mentioning is achieving superheated vapor with temperature above 100 °C using SWE devices, which could open up the possibility of using SWE for sterilization purposes—a promising niche application in underdeveloped areas where energy infrastructure is lacking and inaccessibility to clean water is causing health issues. Producing superheated vapor

with temperature above 100 °C cannot be realized via simply heating up the solar absorber exposed to 1 atm because water boils at 100 °C, which pins the surface water at this temperature as long as liquid water keeps replenishing the evaporation. Vapor above the liquid water surface will always have a lower temperature than the liquid due to thermal resistance presented by the liquid–vapor interfacial region. Superheating the vapor above 100 °C is not possible unless additional heat can be added to the vapor. To achieve this additional heating, Copper et al.[6] leveraged thermal radiation in the infrared wavelength that could be absorbed by water (Figure 8a). Such a strategy was able to superheat water vapor to 133 °C, right above the 132 °C required for sterilization.[210] A key innovation was isolating the solar absorber by a gas gap; therefore, it is not in direct contact with liquid water, which could have cooled the absorber rapidly. Because of this, the solar absorber reached a temperature of ~175 °C, and the thermal emitter heated by the absorber via conduction reached ~150 °C. The radiative heat transfer from the emitter to the water heated it up beyond the boiling point of water (100 °C). In another study, Wang et al.[148] reported vapor generation with a temperature higher than 100 °C under 1 sun using a coiled copper tube coated with black copper oxide as the solar absorber (Figure 8b). Water wicked into the heated tube evaporated within a short distance after entering, and the vapor was then in direct contact with the hot tube wall, continuing to be heated. It needed either a long tube or a higher solar concentration to sufficiently heat up the vapor to reach the superheated state. Due to the low heat transfer efficiency to vapor, the overall solar-to-vapor efficiencies in both studies were relatively low—up to 39%[6] and 27%,[148] respectively. Although Copper's work showed a higher efficiency, they needed more time (1 h) than Wang's strategy (20 min) to achieve superheat.

Condensation Heat Reuse. From eq 1, we can calculate the upper limit of water production from SWE devices to be ~1.4 L/h for a 1 m² solar absorber surface by considering 100% solar-to-vapor efficiency. This is a very low production rate compared to state-of-the-art water treatment methods with the same footprint. However, this limit is based on the assumption that vaporized water takes away all of the latent heat and releases it to the environment as it condenses. State-of-the-art thermal desalination plants are able to make desalinated water economically viable largely because of the reuse of the condensation heat for preheating feedwater, which lowered the overall energy needed per unit water produced. We have seen an innovative design of condensation heat reuse for SWE devices. Chiavozzo et al.[211] presented a passive multistage and low-cost SWE device, where a multistage heat exchanger between the condenser and evaporator was realized in a compact design (Figure 8c). We note that this design is essentially a membrane distillation system, where the temperature difference across a hydrophobic membrane drives the solar-heated feedwater from one side of the membrane to transport as vapor into the other side. When the vapor condensed on the other side of the membrane, latent heat was released, which was used to heat another stream of feedwater for another stage of membrane distillation.[211] With this heat reuse, they demonstrated that ~2 L/m² of water could be produced hourly using a 10-stage system. If we use eq 1, this would translate to an efficiency of ~140%, implying a heat exchange efficiency around 30%. In the state-of-the-art multistage flash (MSF) desalination plants, heat reuse is realized by many stages of heat exchangers (21–40 stages),[212] leading to a thermal energy consumption of ~90 kJ/L for water production.[213] This translates to an efficiency of ~2800% per the definition in eq 1, meaning an overall heat reuse efficiency of >96%. While heat reuse in SWE devices is at its infancy of development, there is still enormous room for its improvement if using the state-of-the-art MSF process as a reference. We also believe that much knowledge can be leveraged from the condensation heat transfer research[214] toward heat exchanger designs for SWE systems.

We would also like to mention that solar–thermal membrane distillation has attracted significant interest in recent years.[215−218] Being a low-temperature process that also promises to leverage low or nonconcentrating solar energy, strategies like heat localization to enlarge the temperature difference across the hydrophobic membrane,[219] latent heat harvesting,[217] and commercial scale membrane structure design[218] have been studied for solar–thermal membrane distillation. Without latent heat reuse, the efficiencies (~21%),[219] however, are significantly lower than those of SWE, mostly due to heat carried away by the liquid stream. With latent heat reuse, the efficiencies are improved significantly to 72% in ref 217 and 140% in ref 211. We refer readers to a few reviews on this topic.[220,221,225]

Lowered Latent Heat in Nanomaterials. If heat reuse reduces the nominal thermal energy needed to evaporate a unit volume of water, lowering the latent heat of vaporization can reduce the actual thermal energy required to evaporate water. In a recent publication, Zhao et al.[222] reported a water production rate of 3.2 L/h per 1 m² of solar absorber surface using a SWE device without heat reuse. This rate is much higher than the upper limit set by eq 1 (1.4 L/m²h). The authors attributed this high production rate to the reduction of water latent heat in the nanostructured molecular hydrogel meshes used in their SWE structure (Figure 8d). The nominal latent heat was reduced to as low as 1000 kJ/kg—only ~40% of the value of bulk water. If verified, this can be extremely intriguing as so many aspects of human activities depend on water evaporation, and reducing water latent heat can enormously impact the energy consumption at a global scale. However, the underlying mechanism has yet to be convincingly explained. Zhao et al.[222] explained their astonishing 60% reduction in water latent heat as water being evaporated as a small cluster instead of individual molecules. Then, fewer hydrogen bonds needed to be broken by thermal energy to break apart the same amount of water molecules. However, it is not clear why water preferred to escape in clusters than as individual molecules in their nanoporous meshes. The authors cited two studies[226,227] on water clusters in the vapor phase, but these studies were on infrared spectroscopic characterization of water clusters of different sizes coordinated around protons or phenols. However, water clusters naturally exist in vapor,[228] and the obvious change in latent heat would require a significant increase in the population of these clusters compared to molecular water in vapor. A follow-up study on the size and population of water clusters in the vapor generated in ref 222 will answer many open questions. Another way to verify the reduced latent heat would be measuring the heat of condensation of the generated vapor, which should exhibit lower-than-normal values. Previous studies[229] indeed showed that water in hydrophobic polymer matrixes tend to form clusters, but the hydrogel developed by Zhao et al.[222] seemed to be hydrophilic. The water-spreading ability of the

hydrophilic surface would help quickly coalescence small clusters into continuous water films. The ability to reduce latent heat by materials design can be an important scientific breakthrough if it can be verified and understood, but there are a lot of fundamental questions to be answered.

> SWE will be more suitable for niche applications in low-resource settings.

Outlook. To summarize, we have seen a rapid increase of research interest surrounding SWE with no or low solar concentrations in the past 5 years. We believe such interest is driven by attractive potential applications of such devices that fit right into the discussion of the water–energy nexus on a global scale. We have witnessed a large wave of material and structure innovations for solar absorbers and thermal management to maximize the solar-to-thermal conversion and minimize the energy loss to the environment so as to optimize the overall solar-to-vapor conversion efficiency. The overall solar-to-vapor efficiencies are now routinely above 80%, with some reaching over 95%. Demonstrations of solar distillation desalination have been a major targeted application, but other types of water treatment, like heavy metal removal and wastewater purification, are also explored. To the best of our knowledge, no SWE devices have made it to the commercialization stage yet, and there are still a lot of technical challenges to be tackled before reaching practical deployment. Among them, we believe that cost, low water production rate, and device reliability due to fouling are major obstacles. It is our feeling that it will be hard for SWE devices to compete with the start-of-the-art reverse osmosis or thermal distillation water treatment plants in terms of economy and throughput, especially at the medium or large scale. In these scales, costs are driven down largely due to energy reuse (e.g., pressure recovery in reverse osmosis and heat recovery in MSF) and centralized pretreatment processes, which can be expensive for SWE devices that are destined to be in distributed small scales due to the low energy density.

> Applied research aimed to enable commercialization of SWE and fundamental research for scientific breakthrough are expected to be the two future directions in the SWE field.

However, we have seen interesting innovations, such as superheated vapor generation[6,148] and passive heat reuse,[211] that can potentially lead to niche applications in low-resource settings. We believe that these are directions deserving further exploration. Another aspect that needs attention is fouling mitigation, especially for biofouling. The solution can be from either novel antifouling materials development or leveraging knowledge from the membrane field[230] because one can always place an antifouling membrane at the inlet of the feedwater for SWE devices. Besides engineering, we believe that fundamental physics involved in SWE is equally important. The implication of significant latent heat reduction in porous materials[222] is extremely intriguing given its potential impact beyond the SWE field, but the observation needs to be further verified, and there are a lot of fundamental questions to be answered. Overall, it is our feeling that the emphasis on the fundamental

science is not sufficient in the SWE field, but as the low-hanging fruits are gone, publishing high-impact papers will become increasingly difficult. It is hopeful that researchers will start to dig deeper into the physics, which may lead to more impactful discoveries to benefit the SWE and its relevant fields. We see the understanding of the molecular level phase transition in confined space as being one of such important directions.[223,224] However, we do not need to recreate the wheel because much knowledge from fields like heat transfer (e.g., phase change heat transfer) and chemistry (e.g., antifouling) can be leveraged.

> Innovations like enabling superheated vapor and condensation heat reuse can help SWE realize niche applications.

In short, we believe that much work still remains to be done in the SWE field, but refocusing efforts on more applied research aimed to enable the eventual commercial adaption of this technology or more fundamental research that may lead to new scientific breakthrough is needed to further advance this field.

■ AUTHOR INFORMATION

Corresponding Authors

Zhiguo Qu − *Xi'an Jiaotong University, Xi'an, China*; Email: zgqu@xjtu.edu.cn

Eungkyu Lee − *University of Notre Dame, Notre Dame, Indiana*; orcid.org/0000-0002-0211-0727; Email: elee18@nd.edu

Tengfei Luo − *University of Notre Dame, Notre Dame, Indiana, and Center for Sustainable Energy at Notre Dame, Notre Dame, Indiana*; orcid.org/0000-0003-3940-8786; Email: tluo@nd.edu

Other Authors

Yunsong Pang − *University of Notre Dame, Notre Dame, Indiana*; orcid.org/0000-0003-0522-4292

Jiajia Zhang − *Xi'an Jiaotong University, Xi'an, China*

Ruimin Ma − *University of Notre Dame, Notre Dame, Indiana*; orcid.org/0000-0003-1527-9289

Complete contact information is available at:
https://pubs.acs.org/10.1021/acsenergylett.9b02611

Biographies

Yunsong Pang is a Ph.D. student at the University of Notre Dame, majoring in Aerospace and Mechanical Engineering. His research interests mainly focus on solar–thermal water evaporation, thermal engineering, and materials development.

Jiajia Zhang is a Ph.D. student in the School of Energy and Power Engineering at Xi'an Jiaotong University. Her research is mainly focusing on solar energy utilization, like plasmonic solar cells, concentration photovoltaic–thermal application, and nanofluids for solar–thermal conversion.

Ruimin Ma is a Ph.D. student in Aerospace and Mechanical Engineering at the University of Notre Dame. His research is mainly focusing on machine learning-related topics, like material informatics, text mining, and natural language processing.

Zhiguo Qu completed his Ph.D degree in 2005 in Engineering Thermophysics at Xi'an Jiaotong University, where he is currently a professor. His research interests cover a wide spectrum in multiscale transport phenomena and energy conversion including solar energy utilization, electrokinetic energy conversion, fuel cells, and thermal management.

Eungkyu Lee earned his Ph.D. degree in Nano Science and Technology at Seoul National University. He joined the University of Notre Dame in 2015 and is currently a Research Assistant Professor. His research is on nanoscale interfacial phenomena, mainly focusing on light–matter interaction for nanoscale materials and photon energy conversion processes.

Tengfei Luo completed his Ph.D. in Mechanical Engineering at Michigan State University. After postdoctoral research at MIT, he joined the University of Notre Dame in 2012, where he is currently the Dorini Family Associate Professor. His research interests span a broad spectrum in multiscale thermal transport, optothermofluids, and water treatment. (https://memt.nd.edu)

■ ACKNOWLEDGMENTS

■ REFERENCES

(1) Mehos, M.; et al. *Concentrating Solar Power Gen3 Demonstration Roadmap*; **2017**. DOI: 10.2172/1338899

(2) Sharshir, S. W.; Peng, G.; Elsheikh, A. H.; Eltawil, M. A.; Elkadeem, M. R.; Dai, H.; Zang, J.; Yang, N. Influence of basin metals and novel wick-metal chips pad on the thermal performance of solar desalination process. *J. Cleaner Prod.* **2019**, 119224.

(3) Al-Karaghouli, A.; Renne, D.; Kazmerski, L. L. Solar and wind opportunities for water desalination in the Arab regions. *Renewable Sustainable Energy Rev.* **2009**, *13*, 2397−2407.

(4) Sharshir, S. W.; Peng, G.; Wu, L.; Essa, F. A.; Kabeel, A. E.; Yang, N. The effects of flake graphite nanoparticles, phase change material, and film cooling on the solar still performance. *Appl. Energy* **2017**, *191*, 358−366.

(5) Sharshir, S. W.; Peng, G.; Wu, L.; Yang, N.; Essa, F. A.; Elsheikh, A. H.; Mohamed, S. I. T.; Kabeel, A. E. Enhancing the solar still performance using nanofluids and glass cover cooling: Experimental study. *Appl. Therm. Eng.* **2017**, *113*, 684−693.

(6) Cooper, T. A.; et al. Contactless steam generation and superheating under one sun illumination. *Nat. Commun.* **2018**, *9*, 5086.

(7) Neumann, O.; et al. Solar Vapor Generation Enabled by Nanoparticles. *ACS Nano* **2013**, *7*, 42−49.

(8) Ghasemi, H.; et al. Solar steam generation by heat localization. *Nat. Commun.* **2014**, *5*, 4449.

(9) Bauer, D.; et al. The water-energy nexus: Challenges and opportunities. *US Department of Energy*; **2014**.

(10) Kahrl, F.; Roland-Holst, D. China's water–energy nexus. *Water Policy* **2008**, *10*, 51−65.

(11) Siddiqi, A.; Anadon, L. D. The water–energy nexus in Middle East and North Africa. *Energy Policy* **2011**, *39*, 4529−4540.

(12) Hardy, L.; Garrido, A.; Juana, L. Evaluation of Spain's water-energy nexus. *Int. J. Water Resour. Dev.* **2012**, *28*, 151−170.

(13) Fang, Z.; et al. Evolution of light-induced vapor generation at a liquid-immersed metallic nanoparticle. *Nano Lett.* **2013**, *13*, 1736−1742.

(14) Ni, G.; et al. Volumetric solar heating of nanofluids for direct vapor generation. *Nano Energy* **2015**, *17*, 290−301.

(15) Ni, G.; et al. A salt-rejecting floating solar still for low-cost desalination. *Energy Environ. Sci.* **2018**, *11*, 1510−1519.

(16) Deng, Z.; et al. A Novel Ink-Stained Paper for Solar Heavy Metal Treatment and Desalination. *Solar RRL* **2018**, *2*, 1800073.

(17) Yang, M.; Gao, M.; Hong, M.; Ho, G. W. Visible-to-NIR Photon Harvesting: Progressive Engineering of Catalysts for Solar-Powered Environmental Purification and Fuel Production. *Adv. Mater.* **2018**, *30*, 1802894.

(18) Ding, T.; et al. Hybrid Photothermal Pyroelectric and Thermogalvanic Generator for Multisituation Low Grade Heat Harvesting. *Adv. Energy Mater.* **2018**, *8*, 1802397.

(19) Zhu, L.; Ding, T.; Gao, M.; Peh, C. K. N.; Ho, G. W. Shape Conformal and Thermal Insulative Organic Solar Absorber Sponge for Photothermal Water Evaporation and Thermoelectric Power Generation. *Adv. Energy Mater.* **2019**, *9*, 1900250.

(20) Gao, M.; Zhu, L.; Peh, C. K.; Ho, G. W. Solar absorber material and system designs for photothermal water vaporization towards clean water and energy production. *Energy Environ. Sci.* **2019**, *12*, 841−864.

(21) Bird, R. E.; Hulstrom, R. L.; Lewis, L. J. Terrestrial solar spectral data sets. *Sol. Energy* **1983**, *30*, 563.

(22) Zhu, L.; Gao, M.; Peh, C. K. N.; Ho, G. W. Recent progress in solar-driven interfacial water evaporation: Advanced designs and applications. *Nano Energy* **2019**, *57*, 507−518.

(23) Wang, A.; et al. Pathways and challenges for efficient solar-thermal desalination. *Sci. Adv.* **2019**, *5*, eaax0763.

(24) Peng, G., Sharshir, S. W., Wang, Y., An, M., Kabeel, A. E., Zang, J., Zhang, L.; Yang, N. Micro/nanomaterials for improving solar still and solar evaporation—A review. *arXiv:1906.08461*; **2019**.

(25) Tao, P.; et al. Solar-driven interfacial evaporation. *Nature energy* **2018**, *3*, 1031−1041.

(26) Liu, H.; Huang, Z.; Liu, K.; Hu, X.; Zhou, J. Interfacial Solar-to-Heat Conversion for Desalination. *Adv. Energy Mater.* **2019**, *9*, 1900310.

(27) Zhou, L.; Li, X.; Ni, G. W.; Zhu, S.; Zhu, J. The revival of thermal utilization from the Sun: interfacial solar vapor generation. *National Science Review* **2019**, *6*, 562−578.

(28) Jin, H.; Lin, G.; Bai, L.; Zeiny, A.; Wen, D. Steam generation in a nanoparticle-based solar receiver. *Nano Energy* **2016**, *28*, 397−406.

(29) Zielinski, M. S.; et al. Hollow mesoporous plasmonic nanoshells for enhanced solar vapor generation. *Nano Lett.* **2016**, *16*, 2159−2167.

(30) Wang, H.; Miao, L.; Tanemura, S. Morphology Control of Ag Polyhedron Nanoparticles for Cost-Effective and Fast Solar Steam Generation. *Solar RRL* **2017**, *1*, 1600023.

(31) Li, H.; He, Y.; Liu, Z.; Huang, Y.; Jiang, B. Synchronous steam generation and heat collection in a broadband Ag@ TiO2 core−shell nanoparticle-based receiver. *Appl. Therm. Eng.* **2017**, *121*, 617−627.

(32) Ishii, S.; Sugavaneshwar, R. P.; Nagao, T. Titanium nitride nanoparticles as plasmonic solar heat transducers. *J. Phys. Chem. C* **2016**, *120*, 2343−2348.

(33) Wang, X.; et al. Direct vapor generation through localized solar heating via carbon-nanotube nanofluid. *Energy Convers. Manage.* **2016**, *130*, 176−183.

(34) Wang, X.; Ou, G.; Wang, N.; Wu, H. Graphene-based recyclable photo-absorbers for high-efficiency seawater desalination. *ACS Appl. Mater. Interfaces* **2016**, *8*, 9194−9199.

(35) Fu, Y.; et al. Investigation on enhancing effects of Au nanoparticles on solar steam generation in graphene oxide nanofluids. *Appl. Therm. Eng.* **2017**, *114*, 961−968.

(36) Scaffardi, L. B.; Pellegri, N.; Sanctis, O. d.; Tocho, J. O. Sizing gold nanoparticles by optical extinction spectroscopy. *Nanotechnology* **2005**, *16*, 158−163.

(37) Neumann, O.; et al. Compact solar autoclave based on steam generation using broadband light-harvesting nanoparticles. *Proc. Natl. Acad. Sci. U. S. A.* **2013**, *110*, 11677−11681.

(38) Cole, J. R.; Halas, N. J. Optimized plasmonic nanoparticle distributions for solar spectrum harvesting. *Appl. Phys. Lett.* **2006**, *89*, 153120.

(39) Sasikumar, K.; Liang, Z.; Cahill, D. G.; Keblinski, P. Curvature induced phase stability of an intensely heated liquid. *J. Chem. Phys.* **2014**, *140*, 234506.

(40) Lombard, J.; Biben, T.; Merabia, S. Kinetics of Nanobubble Generation Around Overheated Nanoparticles. *Phys. Rev. Lett.* **2014**, *112*, 105701.

(41) Prodan, E.; Radloff, C.; Halas, N. J.; Nordlander, P. A Hybridization Model for the Plasmon Response of Complex Nanostructures. *Science* **2003**, *302*, 419−422.

(42) Wei, X.; Zhang, T.; Luo, T. Thermal Energy Transport across Hard−Soft Interfaces. *ACS Energy Lett.* **2017**, *2*, 2283−2292.

(43) Hogan, N. J.; et al. Nanoparticles Heat through Light Localization. *Nano Lett.* **2014**, *14*, 4640−4645.

(44) Liang, Z.; Sasikumar, K.; Keblinski, P. Liquid Phase Stability Under an Extreme Temperature Gradient. *Phys. Rev. Lett.* **2013**, *111*, 225701.

(45) Schiffbauer, J.; Luo, T. Liquid phase stabilization versus bubble formation at a nanoscale curved interface. *Phys. Rev. E: Stat. Phys., Plasmas, Fluids, Relat. Interdiscip. Top.* **2018**, *97*, 033106.

(46) Metwally, K.; Mensah, S.; Baffou, G. Fluence Threshold for Photothermal Bubble Generation Using Plasmonic Nanoparticles. *J. Phys. Chem. C* **2015**, *119*, 28586−28596.

(47) Lukianova-Hleb, E.; et al. Plasmonic Nanobubbles as Transient Vapor Nanobubbles Generated around Plasmonic Nanoparticles. *ACS Nano* **2010**, *4*, 2109−2123.

(48) Lachaine, R.; Boutopoulos, C.; Lajoie, P.; Boulais, É.; Meunier, M. Rational Design of Plasmonic Nanoparticles for Enhanced Cavitation and Cell Perforation. *Nano Lett.* **2016**, *16*, 3187−3194.

(49) Merabia, S.; Keblinski, P.; Joly, L.; Lewis, L. J.; Barrat, J. Critical heat flux around strongly heated nanoparticles. *Phys. Rev. E* **2009**, *79*, 021404.

(50) Kotaidis, V.; Plech, A. Cavitation dynamics on the nanoscale. *Appl. Phys. Lett.* **2005**, *87*, 213102.

(51) Badenhorst, H. A review of the application of carbon materials in solar thermal energy storage. *Sol. Energy* **2019**, *192*, 35.

(52) Yang, J.; Pang, Y.; Huang, W.; Shaw, S. K.; Schiffbauer, J.; Pillers, M. A.; Mu, X.; Luo, S.; Zhang, T.; Huang, Y.; et al. Functionalized Graphene Enables Highly Efficient Solar Thermal Steam Generation. *ACS Nano* **2017**, *11*, 5510 and others..

(53) Zhou, L.; et al. 3D self-assembly of aluminium nanoparticles for plasmon-enhanced solar desalination. *Nat. Photonics* **2016**, *10*, 393.

(54) Zhou, L.; et al. Self-assembly of highly efficient, broadband plasmonic absorbers for solar steam generation. *Science Advances* **2016**, *2*, No. e1501227.

(55) Liu, C.; et al. High-Performance Large-Scale Solar Steam Generation with Nanolayers of Reusable Biomimetic Nanoparticles. *Advanced Sustainable Systems* **2017**, *1*, 1600013.

(56) Chen, M.; et al. Plasmonic nanoparticle-embedded poly (p-phenylene benzobisoxazole) nanofibrous composite films for solar steam generation. *Nanoscale* **2018**, *10*, 6186−6193.

(57) Kaur, M.; Ishii, S.; Shinde, S. L.; Nagao, T. All-ceramic microfibrous solar steam generator: TiN plasmonic nanoparticle-loaded transparent microfibers. *ACS Sustainable Chem. Eng.* **2017**, *5*, 8523−8528.

(58) Xu, W.; et al. Flexible and salt resistant Janus absorbers by electrospinning for stable and efficient solar desalination. *Adv. Energy Mater.* **2018**, *8*, 1702884.

(59) Wang, J.; et al. High-performance photothermal conversion of narrow-bandgap Ti2O3 nanoparticles. *Adv. Mater.* **2017**, *29*, 1603730.

(60) Günay, A. A.; et al. Optically Transparent Thermally Insulating Silica Aerogels for Solar Thermal Insulation. *ACS Appl. Mater. Interfaces* **2018**, *10*, 12603−12611.

(61) Zhao, L.; et al. Harnessing Heat Beyond 200 °C from Unconcentrated Sunlight with Nonevacuated Transparent Aerogels. *ACS Nano* **2019**, *13*, 7508−7516.

(62) Ni, G.; et al. Volumetric solar heating of nanofluids for direct vapor generation. *Nano Energy* **2015**, *17*, 290−301.

(63) Chen, M.; et al. Plasmonic nanoparticle-embedded poly(p-phenylene benzobisoxazole) nanofibrous composite films for solar steam generation. *Nanoscale* **2018**, *10*, 6186−6193.

(64) Chen, C.; Zhou, L.; Yu, J.; Wang, Y.; Nie, S.; Zhu, S.; Zhu, J. Dual functional asymmetric plasmonic structures for solar water purification and pollution detection. *Nano Energy* **2018**, *51*, 451−456.

(65) Zhou, L.; et al. 3D self-assembly of aluminium nanoparticles for plasmon-enhanced solar desalination. *Nat. Photonics* **2016**, *10*, 393.

(66) Zhu, M.; et al. Plasmonic Wood for High-Efficiency Solar Steam Generation. *Adv. Energy Mater.* **2018**, *8*, 1701028.

(67) Zhang, L.; et al. Plasmonic heating from indium nanoparticles on a floating microporous membrane for enhanced solar seawater desalination. *Nanoscale* **2017**, *9*, 12843−12849.

(68) Ye, M.; et al. Synthesis of Black TiOx Nanoparticles by Mg Reduction of TiO2 Nanocrystals and their Application for Solar Water Evaporation. *Adv. Energy Mater.* **2017**, *7*, 1601811.

(69) Wang, J.; et al. High-Performance Photothermal Conversion of Narrow-Bandgap Ti2O3 Nanoparticles. *Adv. Mater.* **2017**, *29*, 1603730.

(70) Liu, C.; et al. High-Performance Large-Scale Solar Steam Generation with Nanolayers of Reusable Biomimetic Nanoparticles. *Advanced Sustainable Systems* **2017**, *1*, 1600013.

(71) Zhu, L.; Gao, M.; Peh, C. K. N.; Wang, X.; Ho, G. W. Self-Contained Monolithic Carbon Sponges for Solar-Driven Interfacial Water Evaporation Distillation and Electricity Generation. *Adv. Energy Mater.* **2018**, *8*, 1702149.

(72) Kashyap, V.; et al. A flexible anti-clogging graphite film for scalable solar desalination by heat localization. *J. Mater. Chem. A* **2017**, *5*, 15227−15234.

(73) Li, T.; et al. Scalable and Highly Efficient Mesoporous Wood-Based Solar Steam Generation Device: Localized Heat, Rapid Water Transport. *Adv. Funct. Mater.* **2018**, *28*, 1707134.

(74) Yin, Z.; et al. Extremely Black Vertically Aligned Carbon Nanotube Arrays for Solar Steam Generation. *ACS Appl. Mater. Interfaces* **2017**, *9*, 28596−28603.

(75) Ren, H.; et al. Hierarchical Graphene Foam for Efficient Omnidirectional Solar−Thermal Energy Conversion. *Adv. Mater.* **2017**, *29*, 1702590.

(76) Hu, X.; et al. Tailoring Graphene Oxide-Based Aerogels for Efficient Solar Steam Generation under One Sun. *Adv. Mater.* **2017**, *29*, 1604031.

(77) Li, Y.; et al. 3D-Printed, All-in-One Evaporator for High-Efficiency Solar Steam Generation under 1 Sun Illumination. *Adv. Mater.* **2017**, *29*, 1700981.

(78) Yang, Y.; et al. Graphene-Based Standalone Solar Energy Converter for Water Desalination and Purification. *ACS Nano* **2018**, *12*, 829−835.

(79) Li, X.; et al. Graphene oxide-based efficient and scalable solar desalination under one sun with a confined 2D water path. *Proc. Natl. Acad. Sci. U. S. A.* **2016**, *113*, 13953−13958.

(80) Guo, A.; Ming, X.; Fu, Y.; Wang, G.; Wang, X. Fiber-Based, Double-Sided, Reduced Graphene Oxide Films for Efficient Solar Vapor Generation. *ACS Appl. Mater. Interfaces* **2017**, *9*, 29958−29964.

(81) Li, Y.; et al. Graphene oxide-based evaporator with one-dimensional water transport enabling high-efficiency solar desalination. *Nano Energy* **2017**, *41*, 201.

(82) Fu, Y.; et al. Accessible Graphene Aerogel for Efficiently Harvesting Solar Energy. *ACS Sustainable Chem. Eng.* **2017**, *5*, 4665−4671.

(83) Liu, K.; et al. Wood−Graphene Oxide Composite for Highly Efficient Solar Steam Generation and Desalination. *ACS Appl. Mater. Interfaces* **2017**, *9*, 7675−7681.

(84) Wang, G.; et al. Reusable reduced graphene oxide based double-layer system modified by polyethylenimine for solar steam generation. *Carbon* **2017**, *114*, 117.

(85) Wang, G.; et al. Reduced Graphene Oxide—Polyurethane Nanocomposite Foam as a Reusable Photoreceiver for Efficient Solar Steam Generation. *Chem. Mater.* **2017**, *29*, 5629–5635.

(86) Fu, Y.; et al. Oxygen plasma treated graphene aerogel as a solar absorber for rapid and efficient solar steam generation. *Carbon* **2018**, *130*, 250.

(87) Liu, X.; et al. Black titania/graphene oxide nanocomposite films with excellent photothermal property for solar steam generation. *J. Mater. Res.* **2018**, *33*, 674–684.

(88) Finnerty, C.; Zhang, L.; Sedlak, D. L.; Nelson, K. L.; Mi, B. Synthetic Graphene Oxide Leaf for Solar Desalination with Zero Liquid Discharge. *Environ. Sci. Technol.* **2017**, *51*, 11701–11709.

(89) Kim, K.; Yu, S.; An, C.; Kim, S.; Jang, J. Mesoporous Three-Dimensional Graphene Networks for Highly Efficient Solar Desalination under 1 sun Illumination. *ACS Appl. Mater. Interfaces* **2018**, *10*, 15602–15608.

(90) Wang, M.; et al. Bifunctional plasmonic colloidosome/graphene oxide-based floating membranes for recyclable high-efficiency solar-driven clean water generation. *Nano Res.* **2018**, *11*, 3854–3863.

(91) Hao, W.; et al. Crumpled graphene ball-based broadband solar absorbers. *Nanoscale* **2018**, *10*, 6306–6312.

(92) Awad, F. S.; Kiriarachchi, H. D.; AbouZeid, K. M.; Özgür, Ü.; El-Shall, M. Plasmonic Graphene Polyurethane Nanocomposites for Efficient Solar Water Desalination. *ACS Appl. Energy Mater.* **2018**, *1*, 976–985.

(93) Xu, N.; et al. Mushrooms as Efficient Solar Steam-Generation Devices. *Adv. Mater.* **2017**, *29*, 1606762.

(94) Tian, Y.; et al. Beyond lotus: Plasma nanostructuring enables efficient energy and water conversion and use. *Nano Energy* **2019**, *66*, 104125.

(95) Secchi, E.; et al. Massive radius-dependent flow slippage in carbon nanotubes. *Nature* **2016**, *537*, 210.

(96) Wei, X.; Luo, T. Effects of Electrostatic Interaction and Chirality on the Friction Coefficient of Water Flow Inside Single-Walled Carbon Nanotubes and Boron Nitride Nanotubes. *J. Phys. Chem. C* **2018**, *122*, 5131–5140.

(97) Holt, J. K.; et al. Fast Mass Transport Through Sub-2-Nanometer Carbon Nanotubes. *Science* **2006**, *312*, 1034–1037.

(98) Borg, M. K.; Reese, J. M. Multiscale simulation of enhanced water flow in nanotubes. *MRS Bull.* **2017**, *42*, 294–299.

(99) Chang, H.; et al. Highly Reversible and Recyclable Absorption under Both Hydrophobic and Hydrophilic Conditions using a Reduced Bulk Graphene Oxide Material. *Adv. Mater.* **2016**, *28*, 3504–3509.

(100) Li, Y.; et al. 3D-Printed, All-in-One Evaporator for High-Efficiency Solar Steam Generation under 1 Sun Illumination. *Adv. Mater.* **2017**, *29*, 1700981.

(101) Liu, K.; et al. Wood—graphene oxide composite for highly efficient solar steam generation and desalination. *ACS Appl. Mater. Interfaces* **2017**, *9*, 7675–7681.

(102) Li, X.; et al. Graphene oxide-based efficient and scalable solar desalination under one sun with a confined 2D water path. *Proc. Natl. Acad. Sci. U. S. A.* **2016**, *113*, 13953–13958.

(103) Gao, X.; et al. Synthesis of Hierarchical Graphdiyne-Based Architecture for Efficient Solar Steam Generation. *Chem. Mater.* **2017**, *29*, 5777–5781.

(104) Li, T.; et al. Scalable and highly efficient mesoporous wood-based solar steam generation device: localized heat, rapid water transport. *Adv. Funct. Mater.* **2018**, *28*, 1707134.

(105) Ni, G.; et al. Steam generation under one sun enabled by a floating structure with thermal concentration. *Nature Energy* **2016**, *1*, 16126.

(106) Xu, Y.; et al. Origami system for efficient solar driven distillation in emergency water supply. *Chem. Eng. J.* **2019**, *356*, 869–876.

(107) Hong, S.; et al. Nature-Inspired, 3D Origami Solar Steam Generator toward Near Full Utilization of Solar Energy. *ACS Appl. Mater. Interfaces* **2018**, *10*, 28517–28524.

(108) Xu, N.; et al. Mushrooms as Efficient Solar Steam-Generation Devices. *Adv. Mater.* **2017**, *29*, 1606762.

(109) Lin, Y.; et al. Low-cost carbonized kelp for highly efficient solar steam generation. *AIP Adv.* **2019**, *9*, 055110.

(110) Fang, J.; et al. Hierarchical porous carbonized lotus seedpods for highly efficient solar steam generation. *Chem. Mater.* **2018**, *30*, 6217–6221.

(111) Zhu, M.; et al. Carbonized daikon for high efficient solar steam generation. *Sol. Energy Mater. Sol. Cells* **2019**, *191*, 83.

(112) Xiao, C.; et al. Sugarcane-Based Photothermal Materials for Efficient Solar Steam Generation. *Chemistry Select* **2019**, *4*, 7891–7895.

(113) Han, X.; Wang, W.; Zuo, K.; Chen, L.; Yuan, L.; Liang, J.; Li, Q.; Ajayan, P. M.; Zhao, Y.; Lou, J. Bio-derived ultrathin membrane for solar driven water purification. *Nano Energy* **2019**, *60*, 567–575.

(114) Chen, Y.; et al. Self-Floating Carbonized Tissue Membrane Derived from Commercial Facial Tissue for Highly Efficient Solar Steam Generation. *ACS Sustainable Chem. Eng.* **2019**, *7*, 2911–2915.

(115) Zhao, X.; et al. Macroporous three-dimensional MXene architectures for highly efficient solar steam generation. *J. Mater. Chem. A* **2019**, *7*, 10446–10455.

(116) Li, C.; et al. Scalable and robust bilayer polymer foams for highly efficient and stable solar desalination. *Nano Energy* **2019**, *60*, 841.

(117) Xiong, Z.; Zhu, Y.; Qin, D.; Chen, F.; Yang, R. Flexible Fire-Resistant Photothermal Paper Comprising Ultralong Hydroxyapatite Nanowires and Carbon Nanotubes for Solar Energy-Driven Water Purification. *Small* **2018**, *14*, 1803387.

(118) Chen, C.; et al. Highly Flexible and Efficient Solar Steam Generation Device. *Adv. Mater.* **2017**, *29*, 1701756.

(119) Jia, C.; Li, Y.; Yang, Z.; Chen, G.; Yao, Y.; Jiang, F.; Kuang, Y.; Pastel, G.; Xie, H.; Yang, B.; Das, S.; Hu, L. Rich Mesostructures Derived from Natural Woods for Solar Steam Generation. *Joule* **2017**, *1*, 588–599.

(120) Mu, P.; et al. Robust aerogels based on conjugated microporous polymer nanotubes with exceptional mechanical strength for efficient solar steam generation. *J. Mater. Chem. A* **2018**, *6*, 18183–18190.

(121) Guo, D.; Yang, X. Highly efficient solar steam generation of low cost TiN/bio-carbon foam. *Science China Materials* **2019**, *62*, 711–718.

(122) Gao, T.; et al. Architecting a Floatable, Durable, and Scalable Steam Generator: Hydrophobic/Hydrophilic Bifunctional Structure for Solar Evaporation Enhancement. *Small Methods* **2019**, *3*, 1800176.

(123) Chen, J.; et al. Space-Confined Seeded Growth of Black Silver Nanostructures for Solar Steam Generation. *Nano Lett.* **2019**, *19*, 400–407.

(124) Yin, K.; et al. Femtosecond laser induced robust Ti foam based evaporator for efficient solar desalination. *J. Mater. Chem. A* **2019**, *7*, 8361–8367.

(125) Liu, P.; et al. Flame-treated and fast-assembled foam system for direct solar steam generation and non-plugging high salinity desalination with self-cleaning effect. *Appl. Energy* **2019**, *241*, 652.

(126) Liu, Z.; et al. Continuously Producing Watersteam and Concentrated Brine from Seawater by Hanging Photothermal Fabrics under Sunlight. *Adv. Funct. Mater.* **2019**, *29*, 1905485.

(127) Peng, G.; et al. High efficient solar evaporation by airing multifunctional textile. *Int. J. Heat Mass Transfer* **2020**, *147*, 118866.

(128) Yu, Z.; Cheng, S.; Li, C.; Li, L.; Yang, J. Highly Efficient Solar Vapor Generator Enabled by a 3D Hierarchical Structure Constructed with Hydrophilic Carbon Felt for Desalination and Wastewater Treatment. *ACS Appl. Mater. Interfaces* **2019**, *11*, 32038–32045.

(129) Chen, C.; et al. Highly flexible and efficient solar steam generation device. *Adv. Mater.* **2017**, *29*, 1701756.

(130) Jia, C.; et al. Rich mesostructures derived from natural woods for solar steam generation. *Joule* **2017**, *1*, 588–599.

(131) Kim, K.; Yu, S.; An, C.; Kim, S.; Jang, J. Mesoporous three-dimensional graphene networks for highly efficient solar desalination

under 1 sun illumination. *ACS Appl. Mater. Interfaces* **2018**, *10*, 15602−15608.

(132) Liu, H.; et al. High-performance solar steam device with layered channels: artificial tree with a reversed design. *Adv. Energy Mater.* **2018**, *8*, 1701616.

(133) Liu, S.; Huang, C.; Luo, X.; Rao, Z. High-performance solar steam generation of a paper-based carbon particle system. *Appl. Therm. Eng.* **2018**, *142*, 566−572.

(134) Qin, D.; Zhu, Y.; Chen, F.; Yang, R.; Xiong, Z. Self-floating aerogel composed of carbon nanotubes and ultralong hydroxyapatite nanowires for highly efficient solar energy-assisted water purification. *Carbon* **2019**, *150*, 233−243.

(135) Jiang, F.; et al. Lightweight, Mesoporous, and Highly Absorptive All-Nanofiber Aerogel for Efficient Solar Steam Generation. *ACS Appl. Mater. Interfaces* **2018**, *10*, 1104−1112.

(136) Miao, E.; et al. Enhanced solar steam generation using carbon nanotube membrane distillation device with heat localization. *Appl. Therm. Eng.* **2019**, *149*, 1255.

(137) Lin, Y.; et al. Low-cost carbonized kelp for highly efficient solar steam generation. *AIP Adv.* **2019**, *9*, 055110.

(138) Liu, Z.; et al. Extremely Cost-Effective and Efficient Solar Vapor Generation under Nonconcentrated Illumination Using Thermally Isolated Black Paper. *Global Challenges* **2017**, *1*, 1600003.

(139) Hou, B.; et al. Functionalized carbon materials for efficient solar steam and electricity generation. *Mater. Chem. Phys.* **2019**, *222*, 159.

(140) Yang, Y.; et al. Membrane assembled from anti-fouling copper-zinc-tin-selenide nanocarambolas for solar-driven interfacial water evaporation. *Chem. Eng. J.* **2019**, *373*, 955.

(141) Morciano, M.; et al. Efficient steam generation by inexpensive narrow gap evaporation device for solar applications. *Sci. Rep.* **2017**, *7*, 11970.

(142) Zhang, P.; Li, J.; Lv, L.; Zhao, Y.; Qu, L. Vertically Aligned Graphene Sheets Membrane for Highly Efficient Solar Thermal Generation of Clean Water. *ACS Nano* **2017**, *11*, 5087−5093.

(143) Li, X.; et al. Efficiency enhancement on the solar steam generation by wick materials with wrapped graphene nanoparticles. *Appl. Therm. Eng.* **2019**, *161*, 114195.

(144) Yin, X.; et al. Macroporous Double-Network Hydrogel for High-Efficiency Solar Steam Generation Under 1 sun Illumination. *ACS Appl. Mater. Interfaces* **2018**, *10*, 10998−11007.

(145) Yu, S.; et al. The impact of surface chemistry on the performance of localized solar-driven evaporation system. *Sci. Rep.* **2015**, *5*, 13600.

(146) Zhang, Z.; et al. Facile and Scalable Fabrication of Surface-Modified Sponge for Efficient Solar Steam Generation. *ChemSusChem* **2019**, *12*, 426−433.

(147) Li, T.; Fang, Q.; Lin, H.; Liu, F. Enhancing solar steam generation through manipulating the heterostructure of PVDF membranes with reduced reflection and conduction. *J. Mater. Chem. A* **2019**, *7*, 17505−17515.

(148) Wang, X.; et al. Solar-driven high-temperature steam generation at ambient pressure. *Prog. Nat. Sci.* **2019**, *29*, 10.

(149) Chang, C.; et al. Three-Dimensional Porous Solar-Driven Interfacial Evaporator for High-Efficiency Steam Generation under Low Solar Flux. *ACS Omega* **2019**, *4*, 3546−3555.

(150) Li, H.; He, Y.; Hu, Y.; Wang, X. Commercially Available Activated Carbon Fiber Felt Enables Efficient Solar Steam Generation. *ACS Appl. Mater. Interfaces* **2018**, *10*, 9362−9368.

(151) Wang, Z.; et al. Paper-based membranes on silicone floaters for efficient and fast solar-driven interfacial evaporation under one sun. *J. Mater. Chem. A* **2017**, *5*, 16359−16368.

(152) Peng, G.; et al. Low-cost high-efficiency solar steam generator by combining thin film evaporation and heat localization: Both experimental and theoretical study. *Appl. Therm. Eng.* **2018**, *143*, 1079.

(153) Huang, W.; et al. Nature-inspired salt resistant polypyrrole–wood for highly efficient solar steam generation. *Sustainable Energy Fuels* **2019**, *3*, 3000−3008.

(154) Yu, Z.; Cheng, S.; Li, C.; Sun, Y.; Li, B. Enhancing efficiency of carbonized wood based solar steam generator for wastewater treatment by optimizing the thickness. *Sol. Energy* **2019**, *193*, 434−441.

(155) Xiong, Z.; Zhu, Y.; Qin, D.; Chen, F.; Yang, R. Flexible Fire-Resistant Photothermal Paper Comprising Ultralong Hydroxyapatite Nanowires and Carbon Nanotubes for Solar Energy-Driven Water Purification. *Small* **2018**, *14*, 1803387.

(156) Liu, Y.; et al. A Bioinspired, Reusable, Paper-Based System for High-Performance Large-Scale Evaporation. *Adv. Mater.* **2015**, *27*, 2768−2774.

(157) Ma, S.; Qarony, W.; Hossain, M. I.; Yip, C. T.; Tsang, Y. H. Metal-organic framework derived porous carbon of light trapping structures for efficient solar steam generation. *Sol. Energy Mater. Sol. Cells* **2019**, *196*, 36−42.

(158) Zhang, Q.; et al. Vertically Aligned Janus MXene-Based Aerogels for Solar Desalination with High Efficiency and Salt Resistance. *ACS Nano* **2019**, *13*, 13196−13207.

(159) Ni, F.; et al. Micro-/Macroscopically Synergetic Control of Switchable 2D/3D Photothermal Water Purification Enabled by Robust, Portable, and Cost-Effective Cellulose Papers. *ACS Appl. Mater. Interfaces* **2019**, *11*, 15498−15506.

(160) Li, K.; et al. Biomimetic MXene Textures with Enhanced Light-to-Heat Conversion for Solar Steam Generation and Wearable Thermal Management. *Adv. Energy Mater.* **2019**, *9*, 1901687.

(161) Fang, Q.; Li, T.; Lin, H.; Jiang, R.; Liu, F. Highly Efficient Solar Steam Generation from Activated Carbon Fiber Cloth with Matching Water Supply and Durable Fouling Resistance. *ACS Appl. Energy Mater.* **2019**, *2*, 4354−4361.

(162) Sun, L.; Liu, J.; Zhao, Y.; Xu, J.; Li, Y. Highly efficient solar steam generation via mass-produced carbon nanosheet frameworks. *Carbon* **2019**, *145*, 352.

(163) Zhu, B.; et al. Flexible and Washable CNT-Embedded PAN Nonwoven Fabrics for Solar-Enabled Evaporation and Desalination of Seawater. *ACS Appl. Mater. Interfaces* **2019**, *11*, 35005−35014.

(164) He, J.; et al. Scalable fabrication of monolithic porous foam based on cross-linked aromatic polymers for efficient solar steam generation. *Sol. Energy Mater. Sol. Cells* **2019**, *201*, 110111.

(165) Ma, X.; et al. Hierarchical Porous SWCNT Stringed Carbon Polyhedrons and PSS Threaded MOF Bilayer Membrane for Efficient Solar Vapor Generation. *Small* **2019**, *15*, 1900354.

(166) Ma, X.; et al. A robust asymmetric porous SWCNT/Gelatin thin membrane with salt-resistant for efficient solar vapor generation. *Applied Materials Today* **2019**, 100459.

(167) Jiang, Q.; et al. Polydopamine-filled bacterial nanocellulose as a biodegradable interfacial photothermal evaporator for highly efficient solar steam generation. *J. Mater. Chem. A* **2017**, *5*, 18397−18402.

(168) Liu, J.; et al. Simultaneously achieving thermal insulation and rapid water transport in sugarcane stems for efficient solar steam generation. *J. Mater. Chem. A* **2019**, *7*, 9034−9039.

(169) Wu, S.; et al. Multifunctional Solar Waterways: Plasma-Enabled Self-Cleaning Nanoarchitectures for Energy-Efficient Desalination. *Adv. Energy Mater.* **2019**, *9*, 1901286.

(170) Sun, H.; et al. Photothermal Conversion Material Derived from Used Cigarette Filters for Solar Steam Generation. *ChemSusChem* **2019**, *12*, 4257−4264.

(171) Sonntag, R. E.; Borgnakke, C.; Van Wylen, G. J. *Fundamentals of Thermodynamics*; Wiley: Hoboken, NJ, 2002.

(172) Tan, M.; Wang, J.; Song, W.; Fang, J.; Zhang, X. Self-floating hybrid hydrogels assembled with conducting polymer hollow spheres and silica aerogel microparticles for solar steam generation. *J. Mater. Chem. A* **2019**, *7*, 1244−1251.

(173) Antia, D. D. J. Direct Synthesis of Air-Stable Metal Complexes for Desalination (and Water Treatment). *Direct Synthesis of Metal Complexes* **2018**, 341−367.

(174) Armstrong, L. E.; Johnson, E. C. Water Intake, Water Balance, and the Elusive Daily Water Requirement. *Nutrients* **2018**, *10*, 1928.

(175) Xu, J.; Xu, F.; Qian, M.; Li, Z.; Sun, P.; Hong, Z.; Huang, F. Copper nanodot-embedded graphene urchins of nearly full-spectrum solar absorption and extraordinary solar desalination. *Nano Energy* **2018**, *53*, 425−431.

(176) Zhu, G.; Xu, J.; Zhao, W.; Huang, F. Constructing Black Titania with Unique Nanocage Structure for Solar Desalination. *ACS Appl. Mater. Interfaces* **2016**, *8*, 31716−31721.

(177) Yi, L.; Ci, S.; Luo, S.; Shao, P.; Hou, Y.; Wen, Z. Scalable and low-cost synthesis of black amorphous Al-Ti-O nanostructure for high-efficient photothermal desalination. *Nano Energy* **2017**, *41*, 600−608.

(178) Yang, Y.; et al. Two-Dimensional Flexible Bilayer Janus Membrane for Advanced Photothermal Water Desalination. *ACS Energy Lett.* **2018**, *3*, 1165−1171.

(179) Liu, Z.; et al. High-absorption recyclable photothermal membranes used in a bionic system for high-efficiency solar desalination via enhanced localized heating. *J. Mater. Chem. A* **2017**, *5*, 20044−20052.

(180) EPA. Secondary drinking water standards: Guidance for nuisance chemicals. *Drinking Water Contaminants-Standards and Regulations*; **2017**.

(181) Li, X.; et al. Three-dimensional artificial transpiration for efficient solar waste-water treatment. *National Science Review* **2018**, *5*, 70−77.

(182) Lou, J.; et al. Bioinspired Multifunctional Paper-Based rGO Composites for Solar-Driven Clean Water Generation. *ACS Appl. Mater. Interfaces* **2016**, *8*, 14628−14636.

(183) Higgins, M. W.; Shakeel Rahmaan, A.; Devarapalli, R. R.; Shelke, M. V.; Jha, N. Carbon fabric based solar steam generation for waste water treatment. *Sol. Energy* **2018**, *159*, 800−810.

(184) Hao, D.; Yang, Y.; Xu, B.; Cai, Z. Bifunctional Fabric with Photothermal Effect and Photocatalysis for Highly Efficient Clean Water Generation. *ACS Sustainable Chem. Eng.* **2018**, *6*, 10789−10797.

(185) Liu, H.; et al. Narrow bandgap semiconductor decorated wood membrane for high-efficiency solar-assisted water purification. *J. Mater. Chem. A* **2018**, *6*, 18839−18846.

(186) Wu, S.; et al. Spill-SOS: Self-Pumping Siphon-Capillary Oil Recovery. *ACS Nano* **2019**, *13*, 13027.

(187) Yang, P.; et al. Solar-driven simultaneous steam production and electricity generation from salinity. *Energy Environ. Sci.* **2017**, *10*, 1923−1927.

(188) McGinnis, R. L.; McCutcheon, J. R.; Elimelech, M. A novel ammoniaâ€"carbon dioxide osmotic heat engine for power generation. *J. Membr. Sci.* **2007**, *305*, 13.

(189) Lin, S.; Yip, N. Y.; Cath, T. Y.; Osuji, C. O.; Elimelech, M. Hybrid pressure retarded osmosis–membrane distillation system for power generation from low-grade heat: Thermodynamic analysis and energy efficiency. *Environ. Sci. Technol.* **2014**, *48*, 5306−5313.

(190) Luo, T.; Luo, S. *Electricity generation from low grade waste heat*; **2019**.

(191) Tamburini, A.; et al. Reverse electrodialysis heat engine for sustainable power production. *Appl. Energy* **2017**, *206*, 1334.

(192) Ding, T.; et al. All-Printed Porous Carbon Film for Electricity Generation from Evaporation-Driven Water Flow. *Adv. Funct. Mater.* **2017**, *27*, 1700551.

(193) Gao, M.; Connor, P. K. N.; Ho, G. W. Plasmonic photothermic directed broadband sunlight harnessing for seawater catalysis and desalination. *Energy Environ. Sci.* **2016**, *9*, 3151−3160.

(194) Gao, M.; Peh, C. K.; Phan, H. T.; Zhu, L.; Ho, G. W. Solar Absorber Gel: Localized Macro-Nano Heat Channeling for Efficient Plasmonic Au Nanoflowers Photothermic Vaporization and Triboelectric Generation. *Adv. Energy Mater.* **2018**, *8*, 1800711.

(195) Neumann, O.; et al. Combining Solar Steam Processing and Solar Distillation for Fully Off-Grid Production of Cellulosic Bioethanol. *ACS Energy Lett.* **2017**, *2*, 8−13.

(196) Bilton, A. M.; Wiesman, R.; Arif, A. F. M.; Zubair, S. M.; Dubowsky, S. On the feasibility of community-scale photovoltaic-powered reverse osmosis desalination systems for remote locations. *Renewable Energy* **2011**, *36*, 3246.

(197) Ghermandi, A.; Messalem, R. Solar-driven desalination with reverse osmosis: the state of the art. *Desalin. Water Treat.* **2009**, *7*, 285−296.

(198) Prihasto, N.; Liu, Q.; Kim, S. Pre-treatment strategies for seawater desalination by reverse osmosis system. *Desalination* **2009**, *249*, 308−316.

(199) Nair, M.; Kumar, D. Water desalination and challenges: The Middle East perspective: a review. *Desalin. Water Treat.* **2013**, *51*, 2030−2040.

(200) Gao, F.; Li, W.; Wang, X.; Fang, X.; Ma, M. A self-sustaining pyroelectric nanogenerator driven by water vapor. *Nano Energy* **2016**, *22*, 19−26.

(201) Alotaibi, S.; Ibrahim, O. M.; Luo, S.; Luo, T. Modeling of a continuous water desalination process using directional solvent extraction. *Desalination* **2017**, *420*, 114−124.

(202) Bajpayee, A.; Luo, T. F.; Muto, A.; Chen, G. Very low temperature membrane-free desalination by directional solvent extraction. *Energy Environ. Sci.* **2011**, *4*, 1672−1675.

(203) Luo, T. F.; Bajpayee, A.; Chen, G. Directional solvent for membrane-free water desalination-A molecular level study. *J. Appl. Phys.* **2011**, *110*, 054905.

(204) Alotaibi, S.; Ibrahim, O. M.; Wang, Y.; Luo, T. Exergy Analysis of Directional Solvent Extraction Desalination Process. *Entropy* **2019**, *21*, 321.

(205) Luo, S.; Pang, Y.; Luo, T. A Continuous Directional Solvent Extraction Desalination Process Realized with the Aid of Electrocoalescence. *Journal of Chemical Engineering & Process Technology* **2018**, *9*, 4.

(206) Alklaibi, A. M.; Lior, N. Membrane-distillation desalination: status and potential. *Desalination* **2005**, *171*, 111−131.

(207) Cabassud, C.; Wirth, D. Membrane distillation for water desalination: how to chose an appropriate membrane? *Desalination* **2003**, *157*, 307−314.

(208) McCutcheon, J. R.; McGinnis, R. L.; Elimelech, M. A novel ammonia—carbon dioxide forward (direct) osmosis desalination process. *Desalination* **2005**, *174*, 1−11.

(209) McGinnis, R. L.; Elimelech, M. Energy requirements of ammonia–carbon dioxide forward osmosis desalination. *Desalination* **2007**, *207*, 370−382.

(210) World Health Organization (WHO). *Best practice guidelines on emergency surgical care in disaster situations*; World Health Organization (WHO), 2005.

(211) Chiavazzo, E.; Morciano, M.; Viglino, F.; Fasano, M.; Asinari, P. Passive solar high-yield seawater desalination by modular and low-cost distillation. *Nature Sustainability* **2018**, *1*, 763−772.

(212) El-Dessouky, H. T.; Ettouney, H. M.; Al-Roumi, Y. Multi-stage flash desalination: present and future outlook. *Chem. Eng. J.* **1999**, *73*, 173−190.

(213) Hoffman, A. R. The connection: water and energy security. *Energy Security*; **2004**, *13*.

(214) Tanasawa, I. *Advances in heat transfer*; Elsevier: Amsterdam, The Netherlands, 1991; pp 55−139.

(215) Dongare, P. D.; et al. Nanophotonics-enabled solar membrane distillation for off-grid water purification. *Proc. Natl. Acad. Sci. U. S. A.* **2017**, *114*, 6936−6941.

(216) Dongare, P. D.; Alabastri, A.; Neumann, O.; Nordlander, P.; Halas, N. J. Solar thermal desalination as a nonlinear optical process. *Proc. Natl. Acad. Sci. U. S. A.* **2019**, *116*, 13182−13187.

(217) Xue, G.; et al. Highly Efficient Water Harvesting with Optimized Solar Thermal Membrane Distillation Device. *Global Challenges* **2018**, *2*, 1800001.

(218) Zaragoza, G.; Andrés-Mañas, J. A.; Ruiz-Aguirre, A. Commercial scale membrane distillation for solar desalination. *npj Clean Water* **2018**, *1*, 20.

(219) Man, S. M. Stats for papers let authors track impact. *Nature* **2011**, *476*, 399−399.

(220) Qtaishat, M. R.; Banat, F. Desalination by solar powered membrane distillation systems. *Desalination* **2013**, *308*, 186.

(221) Khayet, M. Solar desalination by membrane distillation: Dispersion in energy consumption analysis and water production costs (a review). *Desalination* **2013**, *308*, 89.

(222) Zhao, F.; et al. Highly efficient solar vapour generation via hierarchically nanostructured gels. *Nat. Nanotechnol.* **2018**, *13*, 489–495.

(223) Gelb, L. D.; Gubbins, K. E.; Radhakrishnan, R.; Sliwinska-Bartkowiak, M. Phase separation in confined systems. *Rep. Prog. Phys.* **1999**, *62*, 1573–1659.

(224) Lum, K.; Luzar, A. Pathway to surface-induced phase transition of a confined fluid. *Phys. Rev. E: Stat. Phys., Plasmas, Fluids, Relat. Interdiscip. Top.* **1997**, *56*, R6283.

(225) Lum, K.; Chandler, D.; Weeks, J. D. Hydrophobicity at small and large length scales. *J. Phys. Chem. B* **1999**, *103*, 4570.

(226) Miyazaki, M.; Fujii, A.; Ebata, T.; Mikami, N. Infrared spectroscopic evidence for protonated water clusters forming nanoscale cages. *Science (Washington, DC, U. S.)* **2004**, *304*, 1134.

(227) Fujii, A.; Mizuse, K. Infrared spectroscopic studies on hydrogen-bonded water networks in gas phase clusters. *Int. Rev. Phys. Chem.* **2013**, *32*, 266–307.

(228) Johansson, E.; Bolton, K.; Ahlström, P. Simulations of vapor water clusters at vapor–liquid equilibrium. *J. Chem. Phys.* **2005**, *123*, 024504.

(229) Fukuda, M. Clustering of water in polyethylene: A molecular-dynamics simulation. *J. Chem. Phys.* **1998**, *109*, 6476–6485.

(230) Jhaveri, J. H.; Murthy, Z. V. P. A comprehensive review on anti-fouling nanocomposite membranes for pressure driven membrane separation processes. *Desalination* **2016**, *379*, 137–154.